The Astronomical Journal, 166:254 (22pp), 2023 December https://doi.org/10.3847/1538-3881/ad03e9
© 2023. The Author(s). Published by the American Astronomical Society.
OPEN ACCESS

Constraining Background N_2 Inventories on Directly Imaged Terrestrial Exoplanets to Rule Out O_2 False Positives

Sawyer Hall[1], Joshua Krissansen-Totton[1,2,3], Tyler Robinson[3,4,5,6], Arnaud Salvador[4,5,6], and Jonathan J. Fortney[1]
[1] Department of Astronomy & Astrophysics, UC Santa Cruz, Santa Cruz, CA 95064, USA; sajhall@ucsc.edu
[2] Department of Earth and Space Sciences, University of Washington, Seattle, WA, USA
[3] NASA Nexus for Exoplanet System Science Virtual Planetary Laboratory, University of Washington, Box 351580, Seattle, WA 98195, USA
[4] Lunar & Planetary Laboratory, University of Arizona, Tucson, AZ 85721, USA
[5] Department of Astronomy and Planetary Science, Northern Arizona University, Flagstaff, AZ 86011, USA
[6] Habitability, Atmospheres, and Biosignatures Laboratory, University of Arizona, Tucson, AZ 85721, USA
Received 2023 April 26; revised 2023 September 30; accepted 2023 October 15; published 2023 November 20

Abstract

Direct imaging spectroscopy with future space-based telescopes will constrain terrestrial planet atmospheric composition and potentially detect biosignature gases. One promising indication of life is abundant atmospheric O_2. However, various non-biological processes could also lead to O_2 accumulation in the atmospheres of potentially habitable planets around Sun-like stars. In particular, the absence of non-condensible background gases such as N_2 could result in appreciable H escape and abiotic O_2 buildup, so identifying background atmosphere composition is crucial for contextualizing any O_2 detections. Here, we perform retrievals on simulated directly imaged terrestrial planets using `rfast`, a new exoplanet atmospheric retrieval suite with direct imaging analysis capabilities. By simulating Earth-analog retrievals for varied atmospheric compositions, cloud properties, and surface pressures, we determine what wavelength range, spectral resolution, and signal-to-noise ratio (S/N) are necessary to constrain background gases' identity and abundance. We find N_2 backgrounds can be uniquely identified with $S/N \sim 20$ observations, provided that wavelength coverage extends beyond $\sim 1.6\ \mu$m to rule out CO-dominated atmospheres. Additionally, there is a low probability of O_2-dominated atmospheres due to an O_2–N_2 degeneracy that is only totally ruled out at $S/N \sim 40$. If wavelength coverage is limited to 0.2–1.1 μm, then although all other cosmochemically plausible backgrounds can be readily excluded, N_2 and CO backgrounds cannot be distinguished. Overall, our simulated retrievals and associated integration time calculations suggest that near-infrared coverage to at least 1.6 μm and apertures approaching 8 m are needed to confidently rule out O_2 biosignature false positives within feasible integration times.

Unified Astronomy Thesaurus concepts: Exoplanet atmospheres (487); Spectroscopy (1558); Telescopes (1689); Astrobiology (74)

1. Introduction

With the Decadal Survey on Astronomy and Astrophysics 2020 prioritizing advances in astrobiology (National Academies of Sciences, Engineering, and Medicine 2021), and the HabEx and LUVOIR teams publishing their final report on their flagship mission concepts (The LUVOIR Team 2019; Gaudi et al. 2020), it is important to consider how future direct imaging telescopes could be optimized to distinguish atmospheric compositions and detect biosignature gases. One promising indication of life on Earth is abundant atmospheric O_2. However, various non-biological processes could also lead to O_2 accumulation in the atmospheres of potentially habitable planets around Sun-like stars (Kleinböhl et al. 2018; Meadows et al. 2018; Krissansen-Totton et al. 2021).

Planets in the habitable zones of M dwarf stars are potentially susceptible to abiotic oxygen buildup for several reasons. First, the elevated far-ultraviolet/near-ultraviolet ratios of their host stars may lead to the accumulation of O_2 generated via CO_2 dissociation (Tian et al. 2014; Gao et al. 2015; Harman et al. 2015). Second, the extended pre-main-sequence phase (exceeding 100 Myr) of M dwarfs may expose habitable zone planets to high bolometric and extreme ultraviolet (XUV) fluxes, potentially resulting in extensive atmospheric O_2 buildup due to H_2O photolysis followed by H escape (Luger & Barnes 2015; Wordsworth et al. 2018; Krissansen-Totton et al. 2022).

However, even planets around F, G, and K stars may be susceptible to abiotic oxygen buildup via secular planetary oxidation (Wordsworth & Pierrehumbert 2014; Kleinböhl et al. 2018; Krissansen-Totton et al. 2021). For planets with substantial atmospheric inventories of non-condensing gases (such as N_2, CO_2, CO), an atmospheric cold trap generally prevents substantial water vapor from reaching the stratosphere (Wordsworth & Pierrehumbert 2014). Consequently, water photolysis and oxygen accumulation following H loss are low. In contrast, small non-condensible background inventories can lead to elevated H_2O abundances in the upper atmosphere, producing significant abiotic O_2 accumulation (Wordsworth & Pierrehumbert 2014).

This O_2 false positive is particularly problematic since it can occur for any stellar type. Indeed, XUV fluxes from more massive stars are large enough (Abrevaya & Thomas 2018) to enable high water photolysis (and H rates) on planets with weak cold traps due to small inventories of non-condensible background gases like N_2. Since anticipating atmospheric inventories from first principles is challenging (Stüeken et al. 2016; Wordsworth 2016; Johnson & Goldblatt 2018; Lammer 2019), the atmospheric abundance of N_2

Original content from this work may be used under the terms of the Creative Commons Attribution 4.0 licence. Any further distribution of this work must maintain attribution to the author(s) and the title of the work, journal citation and DOI.

must be constrained observationally in order to determine whether O_2 in the atmosphere can likely be attributed to remnants of H_2O dissociation and H escape. Constraining the background gas abundance is also crucial for assessing planetary habitability and climate since pressure broadening by N_2 (or CO) may significantly modulate planetary radiation budgets (Goldblatt et al. 2009; Paradise et al. 2021).

Unfortunately, N_2 has no prominent spectral features within the observational wavelength ranges proposed for a future Habitable Worlds Observatory (HWO), which is traditionally envisioned to have a long-wave observable cutoff of 1.8 μm for exoEarths (The LUVOIR Team 2019; Gaudi et al. 2020). In Earth's atmosphere, N_2 does produce N_2–N_2 collision pairs, $(N_2)_2$, which produce a ~35% decrease in flux at 4.15 μm (Schwieterman et al. 2015). Additionally, the 4.3 μm CO_2 bandwidth corresponds to $(N_2)_2$ absorption for atmospheres with N_2 partial pressures above 0.5 bar and significantly widens the band with increasing N_2 abundances (Schwieterman et al. 2015), but neither of these near-infrared (NIR) features will be accessible in HWO reflected light spectra. HITRAN identifies weaker N_2 absorption features at ~1.4 and ~1.09 μm; however, these bands are too weak to be detected by an HWO-type telescope, though they may be more prominent if atmospheric N_2 abundances are very large, a possibility we do not consider here.

Without strong spectral features in the nominal HWO wavelength range, one promising possibility is that N_2 can be inferred via the absence of spectral features from other plausible background gases that *do* absorb between ~0.3 and 1.8 μm such as O_2, H_2O, O_3, CO_2, etc. By analyzing the directly imaged spectra of an exoplanet, we can infer the background gas indirectly via pressure broadening effect on other gases and by eliminating all other plausible background constituents via a lack of absorption features. This approach has been demonstrated previously. Feng et al. (2018) generated 3D simulated retrievals on a directly imaged Earth analog and successfully constrained both total atmospheric pressure and absorber mixing ratios for O_2, H_2O, and O_3, thereby implicitly obtaining a constrained N_2 mixing ratio. Specifically, Feng et al. (2018) were able to simulate a forward model of an Earth analog that produced accurate planetary and atmospheric parameters, implying a background of N_2 was constrained, though this was not explicitly quantified in the paper. Similarly, Damiano & Hu (2022) performed simulated reflected light retrievals of terrestrial planets and were able to constrain the main atmospheric component (N_2, O_2, or CO_2) and trace gas mixing ratios (H_2O, O_3, and CH_4) for a variety of atmospheric compositions. Damiano & Hu (2022) reported that optical-only retrievals (0.4–1.0 μm) frequently resulted in incorrect background gas identification, whereas combined optical+NIR retrievals (0.4–1.8 μm) constrained background gases more reliably. Similar techniques have been successfully applied to constrain background gases in simulated retrievals on sub-Neptunes (Damiano & Hu 2021).

However, previous studies have not considered CO backgrounds. This is of particular importance for diagnosing O_2 false positives because whereas abundant N_2 would disfavor abiotic oxygen accumulation due to low non-condensible inventories, a CO-rich background could indicate abiotic O_2 accumulation via CO_2 photodissociation (Zahnle et al. 2008; Gao et al. 2015; Hu et al. 2020). Here, we performed simulated reflected light retrievals to investigate whether non-condensible gas abundances could be constrained and whether non-condensible species could be uniquely identified for an Earth analog. We performed simulated reflected light retrievals on directly imaged terrestrial planets using `rfast`, a new exoplanet atmospheric retrieval suite with direct imaging analysis capabilities (Robinson 2022; Robinson & Salvador 2023). Crucially, we perform retrievals on partial pressures such that all gases are treated equally in our inverse calculations. This ensures that the resultant constraints on background gases are robust and not artifacts of our chosen priors or the initialization of Monte Carlo calculations.

2. Methods

For our simulations, we used the `rfast` retrieval suite, a one- or three-dimensional radiative transfer exoplanetary atmosphere forward model with direct imaging analysis capabilities from Robinson & Salvador (2023), specifically `rfast v2.6.5` (Robinson 2022). To generate synthetic spectra of our modeled exoplanet, `rfast` is equipped with a radiative transfer model that generates a high-resolution spectrum. Molecular opacities in `rfast` are derived from the HITRAN2020 database (Gordon et al. 2022) using the Line-By-Line ABsorption Coefficients tool, LBLABC (Meadows & Crisp 1996). The spectrum resolution is then degraded to match the resolution specified via an instrument model. Our retrievals were based on reflected light spectroscopy at full phase. To optimize the retrieval process, `rfast` is nearly entirely written using linear algebra techniques to take advantage of vectorized computational methods, the exceptions being atmospheric recursion relations and integration in the three-dimensional reflected light option. We also made use of `rfast`'s water ice/liquid cloud coverage modeling designed with realistic wavelength-dependent scattering properties and a Henyey–Greenstein phase function. Further notable `rfast` capabilities include vertically varying gas, temperature, and atmospheric pressure profiles and the ability to divide a synthetic spectrum into multiple bands with distinct wavelength coverage, noise levels, and spectral resolutions. Here we generated our spectra using a constant error function that generated noise at 1 μm for a given signal-to-noise ratio (S/N) and applied that error to each spectral point.

After generating the noisy exoplanet spectra, `rfast` retrievals are handled via `emcee` Markov Chain Monte Carlo (MCMC) sampler (Foreman-Mackey et al. 2013). `rfast` allows for retrievals of atmospheric, planetary, and orbital parameters with uniform or Gaussian priors in either log or linear space. Here, all 14 retrieved planetary parameters were retrieved in `log10` space (Table 1). Our retrievals included seven unknown atmospheric gas partial pressures: N_2, O_2, H_2O, O_3, CO_2, CH_4, and CO. A `log10` uniform prior is assumed for all constituents ranging from 10^{-2}–10^7 Pa. Note that we are assuming that H_2-dominated atmospheres can be excluded based on contextual information, including the fact that combustible H_2–O_2 atmospheres are kinetically unstable (Grenfell et al. 2018). Yet, our retrievals are agnostic on which of the remaining gases constitutes the dominant background. Our retrievals also include seven unknown planetary parameters: albedo (A_s, prior range 0.01–1.0), planet radius (R_p, prior range $10^{-0.5}$–$10^{0.5}$ $R_\oplus$), planet mass (M_p, prior range 0.1–10 $M_\oplus$), cloud thickness (Δpc, prior range 1–10^7 Pa), cloud top pressure (p_t, prior range 1–10^7 Pa), cloud extinction optical thickness (τ_c, prior range 10^{-3}–10^3), and cloud cover fraction (f_c, prior range 10^{-3}–1). Cloud top pressures below the surface pressure are prohibited. Each retrieval adopted 200 walkers within `emcee` and the walkers' positions were randomly initialized within the parameters' prior ranges. Our

Table 1
Nominal Values of Parameters Retrieved

Parameter Name	Parameter Symbol	True Value (log10)	Prior Range (log10 Uniform)
N_2 abundance (Pa)	N_2	4.896	[−2, 7]
O_2 abundance (Pa)	O_2	4.327	[−2, 7]
H_2O abundance (Pa)	H_2O	2.481	[−2, 7]
O_3 abundance (Pa)	O_3	−1.151	[−2, 7]
CO_2 abundance (Pa)	CO_2	1.606	[−2, 7]
CO abundance (Pa)	CO	−1.996	[−2, 7]
CH_4 abundance (Pa)	CH_4	−0.695	[−2, 7]
Planetary albedo	As	−1.301	[−2, 0]
Planetary radius ($R_\oplus$)	Rp	0.0	[−0.5, 0.5]
Planetary mass ($M_\oplus$)	Mp	0.0	[−1, 1]
Cloud thickness (Pa)	dpc	4.0	[0, 7]
Cloud top pressure (Pa)	pt	4.778	[0, 7]
Cloud extinction optical thickness (Pa)	tauc0	1.0	[−3, 3]
Cloud cover fraction	fc	−0.301	[−3, 0]

Note. If not explicitly stated in the figure, reference parameters' values are the ones defined here.

retrievals had each walker take 200,000 steps with a burn-in of 150,000 and a thinning of 100.

Retrieval parameters and their prior ranges, as well as the *true* values used to generate our nominal synthetic spectrum, are shown in Tables 1 and 2. Partial pressure retrievals avoid biased priors compared to retrievals on mixing ratios. Indeed, for the latter case, an a priori background gas must be assumed with a mixing ratio equal to 1 minus the summation of all other constituents. If the other constituents have uniform priors in log space, then the implied prior for the assumed background gas is skewed heavily toward high values. A partial pressure retrieval is broadly equivalent to retrieving centered log ratios for atmospheric abundances (Benneke & Seager 2012; Damiano & Hu 2021, 2022), except that it removes the need to retrieve total pressure as a separate parameter ($p_{\max}$ is simply the sum of the partial pressures of every gas in the atmosphere) and avoids any potential biases with MCMC chain initialization in centered-log-ratio space.

Table 2 shows our assumed instrument parameters. Nominal retrievals are performed over the full wavelength range (0.2–1.8 μm), with resolutions of 7, 140, and 70 corresponding to the UV (0.2–0.4 μm), optical (0.4–1.0 μm), and NIR (1.0–1.8 μm) portions of the spectrum, respectively. An S/N of 20 was applied at 1.0 μm with constant error bars and then applied across the full wavelength range. S/N = 20 is assumed in all nominal retrievals, but sensitivity tests for S/N = 10 and S/N = 40 are also performed. An isothermal temperature of 294 K is assumed, and the supplementary material shows that reflected light retrievals are largely insensitive to temperatures within the range expected for an Earth analog.

Using our retrieval outputs from `rfast` and `emcee`, we determine what S/N and resolution would be necessary to constrain the non-absorbing atmospheric background's abundance given the HWO wavelength ranges to confidently distinguish O_2 false positives. For a more in-depth analysis of `rfast`'s capabilities, see Robinson & Salvador (2023).

Table 2
Nominal Values of the Instrument Model

Parameter Name	Parameter Symbol	True Value
Short wavelength cutoff (μm)	lams	0.2,0.4,1.0
Long wavelength cutoff (μm)	laml	0.4,1.0,1.8
Spectral resolving power (lam/dlam)	res	7, 140, 70
Signal-to-noise ratio	S/N	20
Wavelength where S/N is Defined	lam0	1.0

Note. If not explicitly stated in the figure, reference instrument model values are the ones defined here and the values shown are in linear space.

We also tested what observation times, telescope diameters, and resolutions would equate to in terms of observational S/Ns at each wavelength. We accomplished this using `coronagraph`, a reflected light coronagraph noise model for directly imaging exoplanets with a coronagraph-equipped telescope with capabilities for transmission and emission spectroscopy noise modeling. The original IDL code for the coronagraph model was developed and published by Robinson et al. (2016), with the expanded model adapted by Lustig-Yaeger et al. (2019).

3. Results

3.1. Forward Modeling

As proof of concept, we used `rfast` to create a synthetic spectrum of our true atmosphere (Table 1) that was then compared to spectra generated with different assumed background gases. Figure 1 shows our nominal (true) N_2-dominated spectrum alongside the same planet with different background gases. For the non-N_2-dominated cases, the 78% N_2 mixing ratio was simply swapped with the alternative background gas. For all plausible alternative background gases (O_2, H_2O, CO_2, CO, CH_4, H_2), there are prominent absorption features in the 0.2–1.8 μm range, the absence of which (alongside pressure broadening) would strongly suggest either an N_2 background gas (or a cosmochemically improbable non-absorbing background such as Ne or Ar—although see the discussion in Section 4 for further consideration of other non-condensibles). Next, we perform simulated retrievals to quantify this result for plausible observational S/N and resolution.

Figure 1 shows there are distinct spectral differences between the spectra of N_2-dominated atmospheres with O_2, H_2O, H_2, CO_2, and CH_4-dominated atmospheres throughout the 0.2–1.8 μm wavelength range. The most notable distinction between N_2-dominated and CO-dominated atmospheres occurs at ∼1.6 μm due to a CO absorption feature. H_2O has multiple visible-NIR absorption features, O_2 has 0.76 μm absorption and smaller NIR O_2–O_2 features, CO_2 has similar 1.2 and 1.6 μm features, and CH_4 has strong absorption throughout the NIR. The opacities in `rfast` assume N_2 broadening since line lists typically do not have data for species other than N_2, air, and/or H_2. In practice, different background gases would have different broadening effects, so the N_2-broadened results here are conservative in that regard.

3.2. Simulated Retrievals

Figure 2 shows the retrieved spectrum from our nominal retrieval alongside the true synthetic spectrum with assumed S/N = 20 error bars. The 95% confidence interval on the

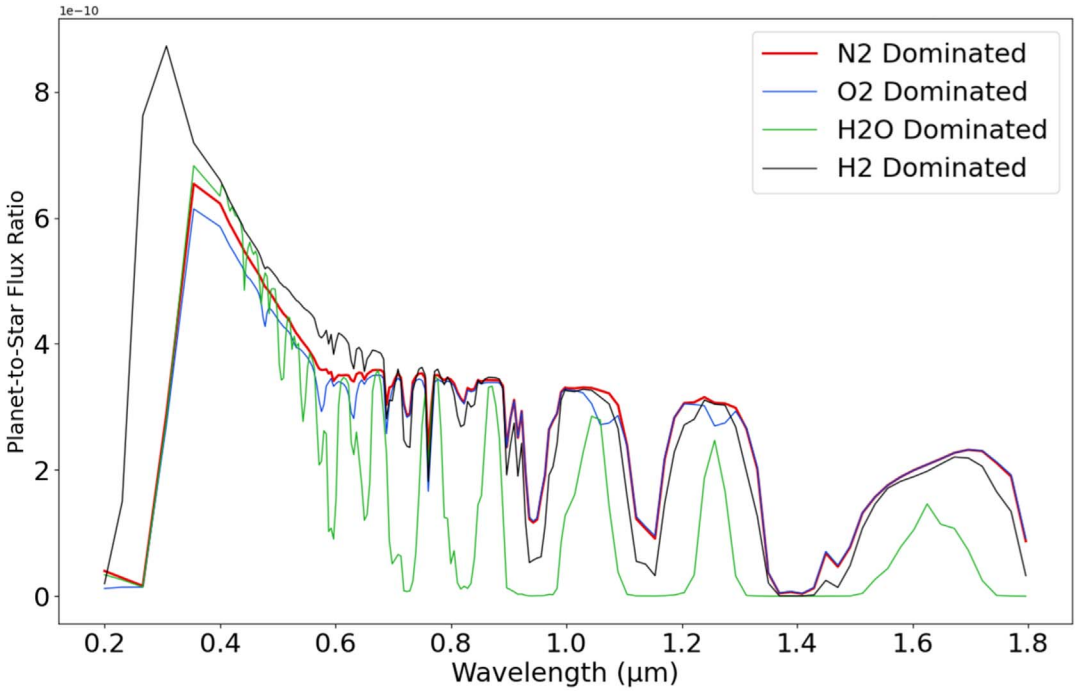

(a) Nominal N_2-Dominated Spectrum vs. Non-Carbon Based Atmospheric Gas Dominated Spectra

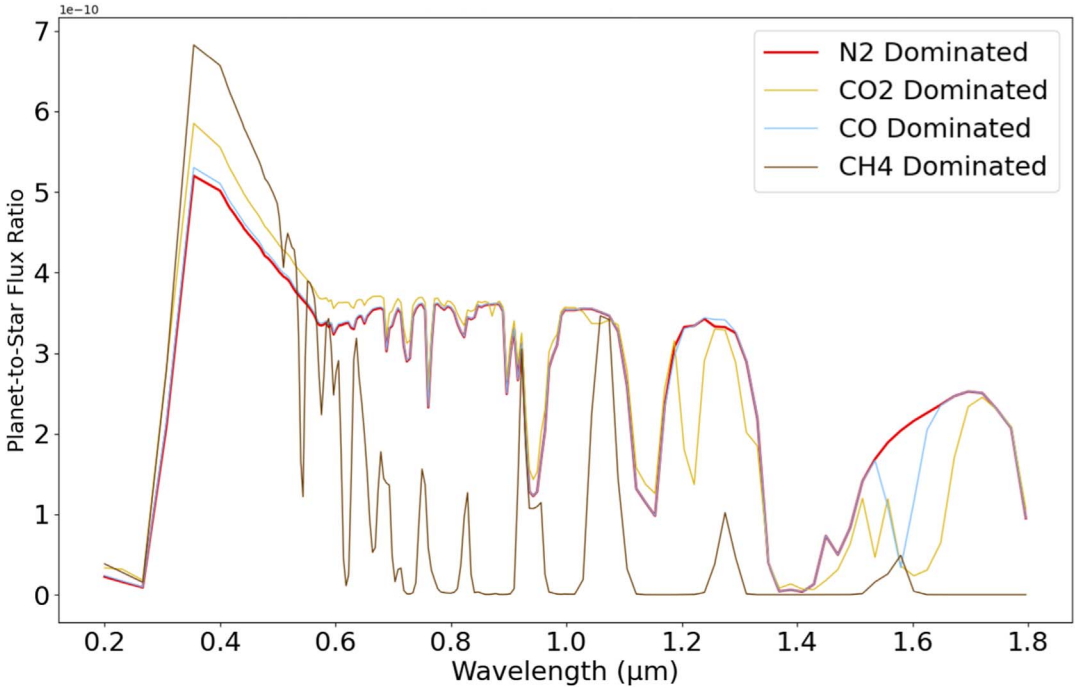

(b) Nominal N_2-Dominated Spectrum vs. Carbon Based Atmospheric Gas Dominated Spectra

Figure 1. Our nominal N_2-dominated model reflectance spectrum compared with spectra generated by swapping atmospheric species abundances with our background N_2 abundance (mixing ratio of 0.78). An Earth-like atmospheric composition is assumed, except for the swapped dominant species. (a) Nominal N_2-dominated spectrum vs. non-carbon-based atmospheric gas-dominated spectra. (b) Nominal N_2-dominated spectrum vs. carbon-based atmospheric gas-dominated spectra.

retrieved spectrum is broadly consistent with the true input spectrum, within error. To generate the confidence interval we sampled 1000 spectra from our posteriors. Additionally, a blue spectrum is overplotted on the confidence interval representing the median (i.e., best-fit) spectrum generated from the spectral confidence interval. Figure 3 shows the corresponding corner plot with posteriors for all retrieved parameters. Every retrieval we ran included the same 14 retrieved parameters, but

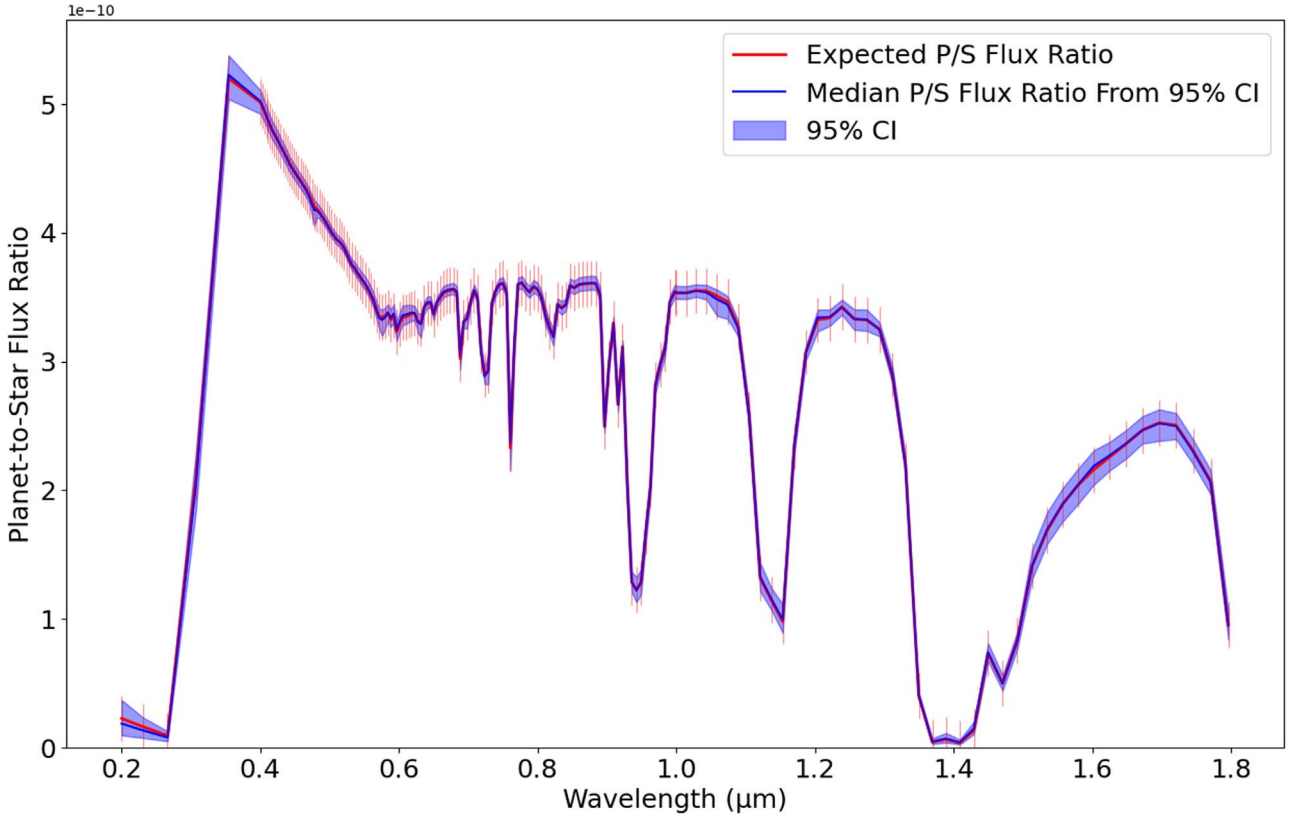

Figure 2. True N_2-dominated planet-to-star flux ratio spectrum with an assumed $S/N = 20$ (red) plotted against 1000 randomly sampled retrieved spectra with 95% confidence intervals. The blue spectrum is the median spectrum created from the 1000 plotted model runs that make up our confidence interval.

subsequent corner plots only show gas abundances for easier viewing. Diagonal elements represent the marginalized posterior distributions for each parameter, whereas off-diagonal elements show the 2D covariance between parameters overplotted with the 1σ, 2σ, and 3σ contours. Along with the parameter name, the 1D parameter posteriors list the median retrieved value with 68% confidence interval uncertainties. Marginalized posteriors also have their parameter's true values (Table 1) overplotted as light blue lines and the dashed lines (left to right) mark the 16%, 50%, and 84% quantiles.

The posteriors in Figure 3 confirm what was suggested by forward modeling, namely, that it is possible to infer the background gas abundance for direct imaging observations of terrestrial exoplanets. For this Earth-analog case, we infer an N_2 background gas with partial pressure $\log_{10}(\mathtt{N_2}) = 4.90^{+0.29}_{-0.43}$, corresponding to $\mathtt{N_2} = 7.94\ ^{+7.54}_{-4.99} \times 10^4$ Pa (68% confidence), or equivalently, a mixing ratio of $10^{-0.15^{+0.08}_{-0.27}} = 0.71^{+0.14}_{-0.32}$, shown in Figure 4. The abundances of O_2, H_2O, and O_3 are tightly constrained, which rules them out as background gases, whereas the absence of CO_2, CO, and CH_4 absorption features places upper limits on their respective abundances that similarly rule them out as dominant background gases. Summing the partial pressures of our retrieved atmospheric species we infer total pressure to be $\log_{10}(\mathtt{pmax}) = 5.07^{+0.24}_{-0.22}$, corresponding to $\mathtt{pmax} = 1.17^{+0.87}_{-0.47} \times 10^5$ Pa (with 68% confidence), meaning an N_2-dominated background is required to fit the observed spectrum. In other words, there is a high probability that the nitrogen partial pressure is a large fraction of the total atmospheric pressure.

The only possible source of ambiguity is a degeneracy between O_2–N_2 backgrounds, which can be seen in the O_2 posterior and corresponding 2D covariant posteriors of Figure 4. This feature arises because O_2 (and O_2–O_2) absorption features are comparatively weak. While the probability of an O_2-dominated atmosphere is low for $S/N = 20$ retrievals, the O_2–N_2 background degeneracy can be resolved by higher S/N observations. See Section 3.5 for detailed information regarding how well our model rules out O_2-dominated atmospheres for different assumed S/Ns.

Importantly, our atmospheric species were retrieved as partial pressures of the total atmosphere, as opposed to retrieving said species as VMRs. Retrieving the gases as partial pressures allowed our atmospheric constituents' values to be explored independently of each other's abundances and avoid any biases from filling the background with a non-absorbing gas. Although both retrieval methods produced results that were superficially consistent with our true spectra and had confidence intervals that fit within error bars, closer investigation revealed that the VMR retrieval approach was biased toward our predefined background gas (see supplementary materials for a comparison between partial pressure and VMR retrievals).

3.3. Simulated Retrievals of CO-dominated Atmospheres

To test whether simulated retrievals can distinguish between N_2-dominated and CO-dominated atmospheres, we repeated the calculation described above except that the true N_2 and CO mixing ratios were exchanged when generating the true synthetic spectrum. Figure 5 shows the results of this retrieval on a 78% CO atmosphere and Figure 6 compares the retrieved gas abundances

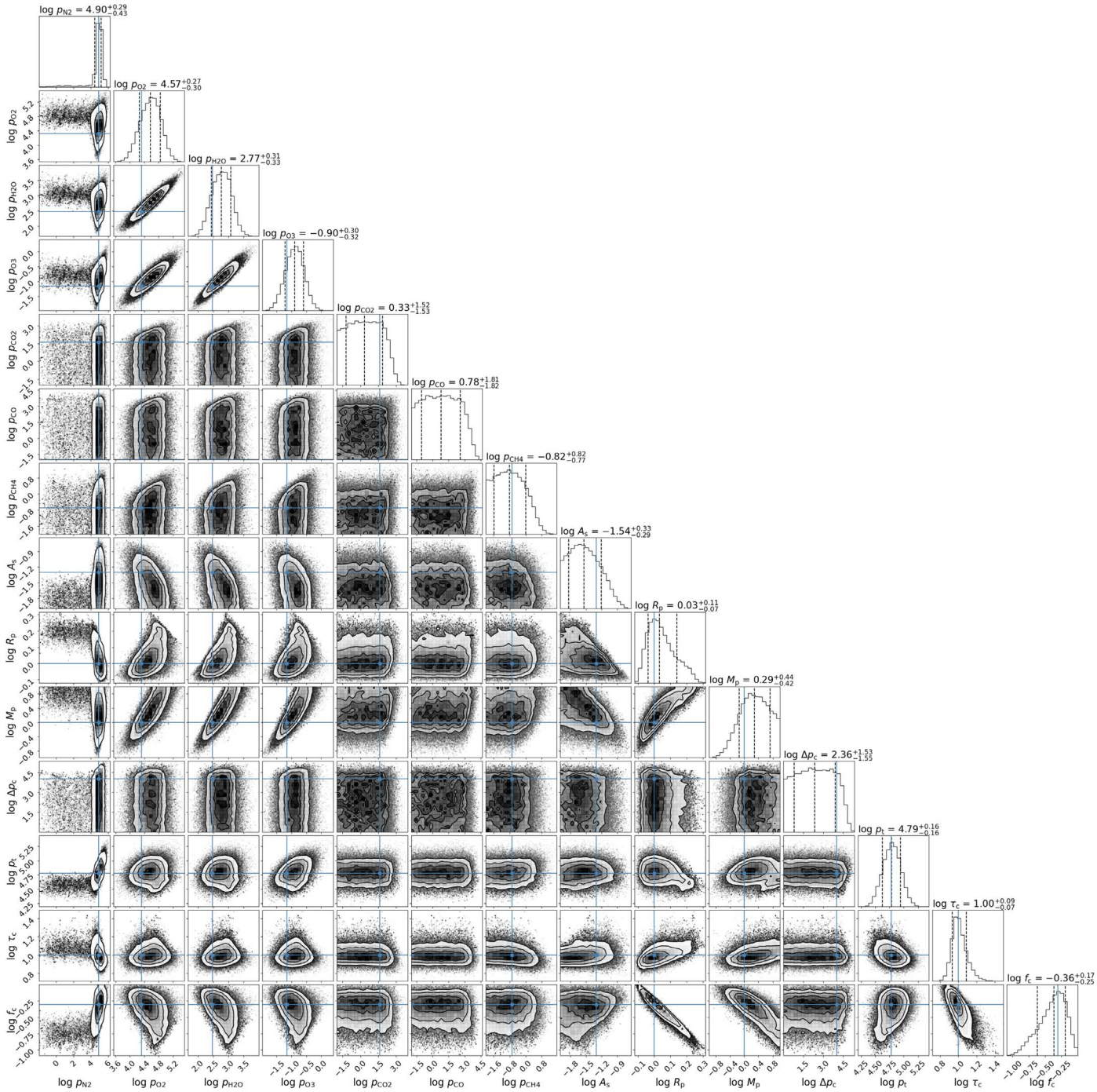

Figure 3. Posterior distributions of our nominal partial pressure retrieval with all retrieved parameters. We retrieved on a wavelength-dependent resolution $R = 7$, 140, 70 at wavelength ranges 0.2–0.4, 0.4–1.0, 1.0–1.8 μm with an assumed S/N of 20 at all wavelengths. The parameters' true values are plotted with light blue lines. The cells off the diagonal are the covariant 2D posterior distributions of their axial posteriors shown with their normal distribution 1σ, 2σ, and 3σ contours. The diagonal parameter posteriors are also plotted with dashed lines (left to right) that mark the 16%, 50%, and 84% quantiles.

for our nominal calculation and CO-dominated retrieval. Figures 6(a) and (b) present the N_2- and CO-dominated partial pressure retrieval results, respectively. The CO background is correctly identified in Figure 6(b), with an abundance of $10^{5.03^{+0.24}_{-0.21}}$ Pa, whereas N_2 maximum abundance is limited to account for CO absorption at 1.6 μm. Constraints on other atmospheric constituents are largely unaffected by switching background gases.

Figure 7 highlights the N_2 and CO posteriors for the two partial pressure retrievals described above. Posteriors from the nominal N_2-dominated atmosphere retrieval are shown in red, and posteriors from the CO-dominated retrieval are shown in blue. The left column shows the retrieved N_2 posteriors for the two retrievals with N_2's true value for each respective retrieval shown with the vertical lines. The right column of Figure 7 illustrates the same for CO abundances, i.e., retrieved CO abundances for both N_2- and CO-dominated retrievals. The top row of Figure 7 shows the retrieved gas partial pressures while the bottom row shows the VMRs of the gases. The posterior distributions demonstrate that both N_2-dominated and CO-dominated atmospheres can be confidently identified.

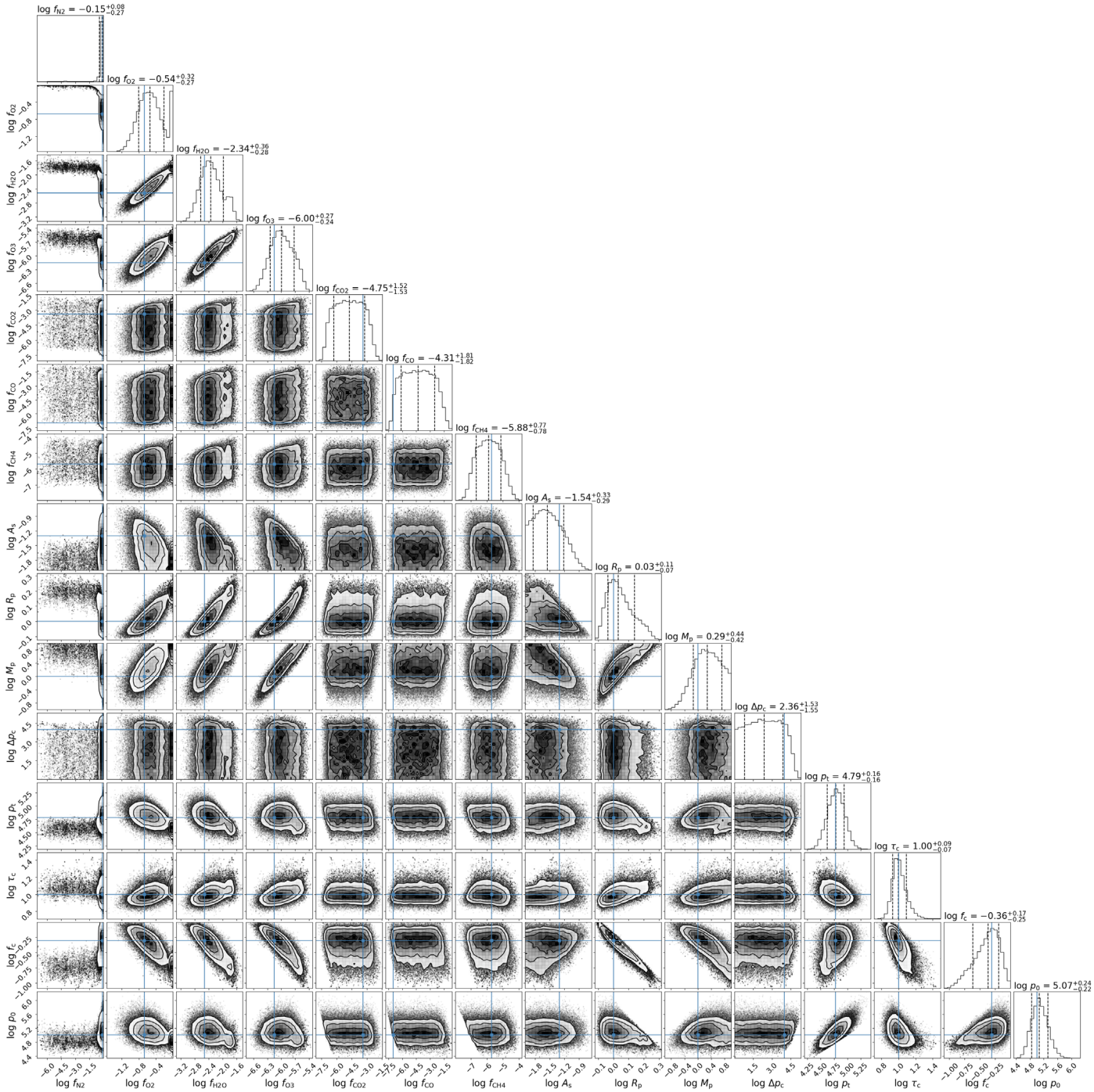

Figure 4. The same retrieval and results as Figure 3 except gas values are represented by volume mixing ratios (VMRs) rather than partial pressures. In addition to presenting the atmospheric gases with their VMR values, the surface pressure is also included with respective correlations in the bottom row.

3.4. Sensitivity to Observational Wavelength Range

The ability to constrain N_2 and CO abundances in the 0.2–1.8 μm wavelength range at $S/N = 20$ is encouraging. However, we also considered restricted wavelength range observations to test the efficacy of a descoped telescope with a wavelength range of 0.2–1.1 μm. Figure 8 shows our full 0.2–1.8 μm range spectrum with N_2–CO abundance tradeoffs, and a highlighted 0.2–1.1 μm range. Crucially, the only spectral feature available to differentiate N_2 from CO within the 0.2–1.1 μm band is the Rayleigh tail differences. However, these differences in spectra are imperceptible to a telescope that would have to filter through realistic noise. Note that N_2 pressure broadening was assumed for all calculations in this study because CO broadening has not yet been experimentally constrained. In practice, CO versus N_2 broadening could help distinguish the two gases, even in the absence of CO absorption features.

All other parameters were held constant for 0.2–1.1 μm retrievals; $R = 7$, 140, and 70 for wavelength ranges of 0.2–0.4 μm, 0.4–1.0 μm, and1.0–1.1 μm, respectively, and a wavelength-independent $S/N = 20$ was assumed. Figure 9 presents the corresponding marginal distributions of N_2 and CO for both the 0.2–1.1 μm cases and the 0.2–1.8 μm cases for

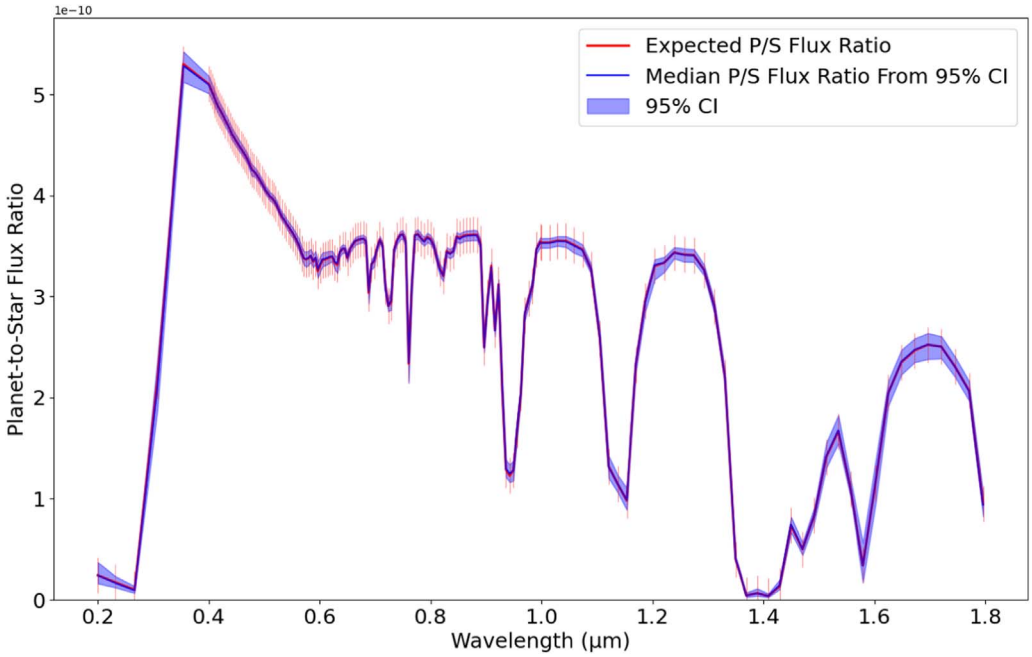

Figure 5. True CO-dominated atmosphere planet-to-star flux ratio spectrum (red) plotted against 1000 randomly sampled retrieved spectra with 95% confidence intervals (blue area).

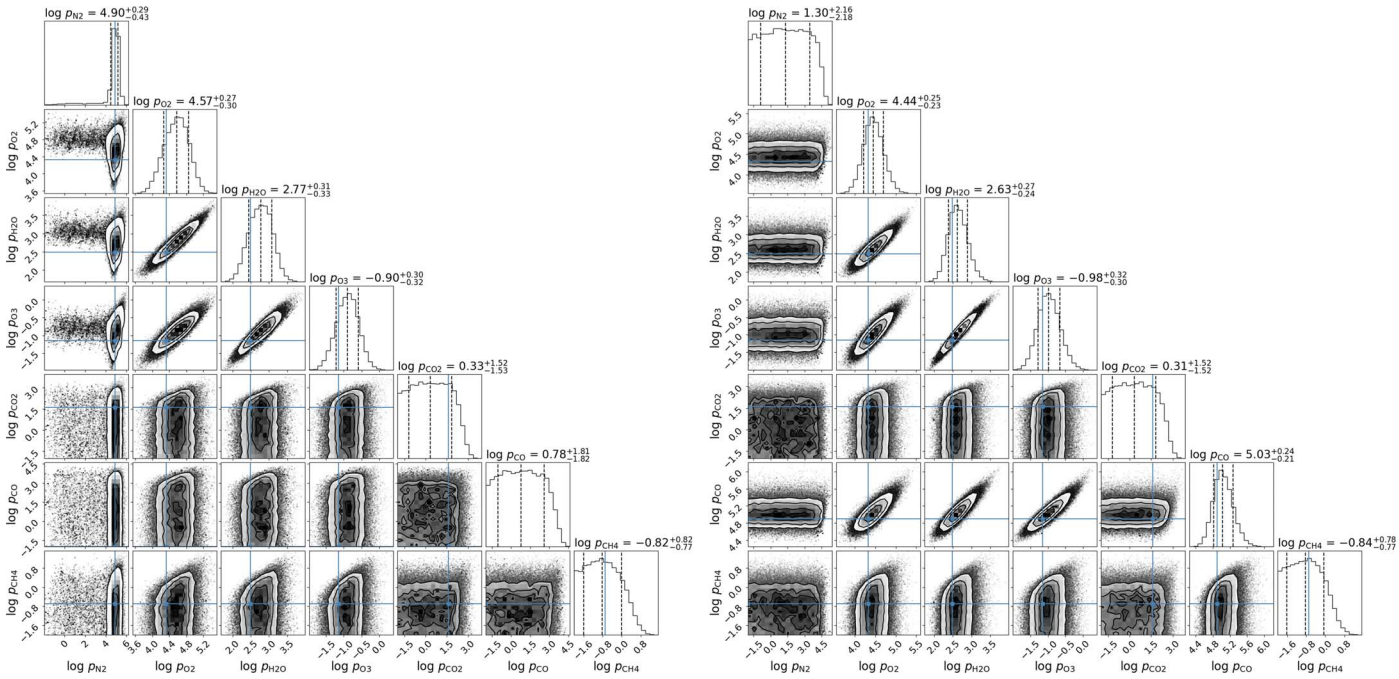

(a) Partial Pressure Gases-Only Corner Plot w/ N_2 as BG (b) Partial Pressure Gases-Only Corner Plot w/ CO as BG

Figure 6. Gas-only corner plots (other retrieved parameters not shown) of our nominal N_2-dominated partial pressure retrieval and the CO-dominated partial pressure retrieval. Gas abundances are represented by their `log10` pressure in Pa. (a) Partial pressure gas-only corner plot w/N_2 as BG. (b) Partial pressure gas-only corner plot w/CO as BG.

comparison and demonstrates our models' abilities to constrain N_2 and CO gas abundances in different wavelength regimes. The left column shows our N_2 abundance posteriors from our nominal and 0.2–1.1 μm retrievals, where N_2 was defined as the background gas for both cases, so they share the same true value. Similarly, the right column shows our CO abundance posteriors from our nominal CO-dominated and 0.2–1.1 μm CO-dominated retrievals, again, both cases shared the same true value. As suggested by Figure 9, restricting the wavelength range omits the prominent 1.6 μm CO absorption feature, and thus N_2-dominated and CO-dominated backgrounds cannot be distinguished. For both N_2-dominated and CO-dominated true spectra, the N_2–CO covariance distribution for the 0.2–1.1 μm retrieval cases are essentially identical and show that neither CO nor N_2 can be confidently and independently detected (see Appendix A.3). Extending observations beyond the 1.6 μm CO absorption feature greatly tightens constraints on N_2 and CO when they are the dominating gas (see the Supplementary Material for

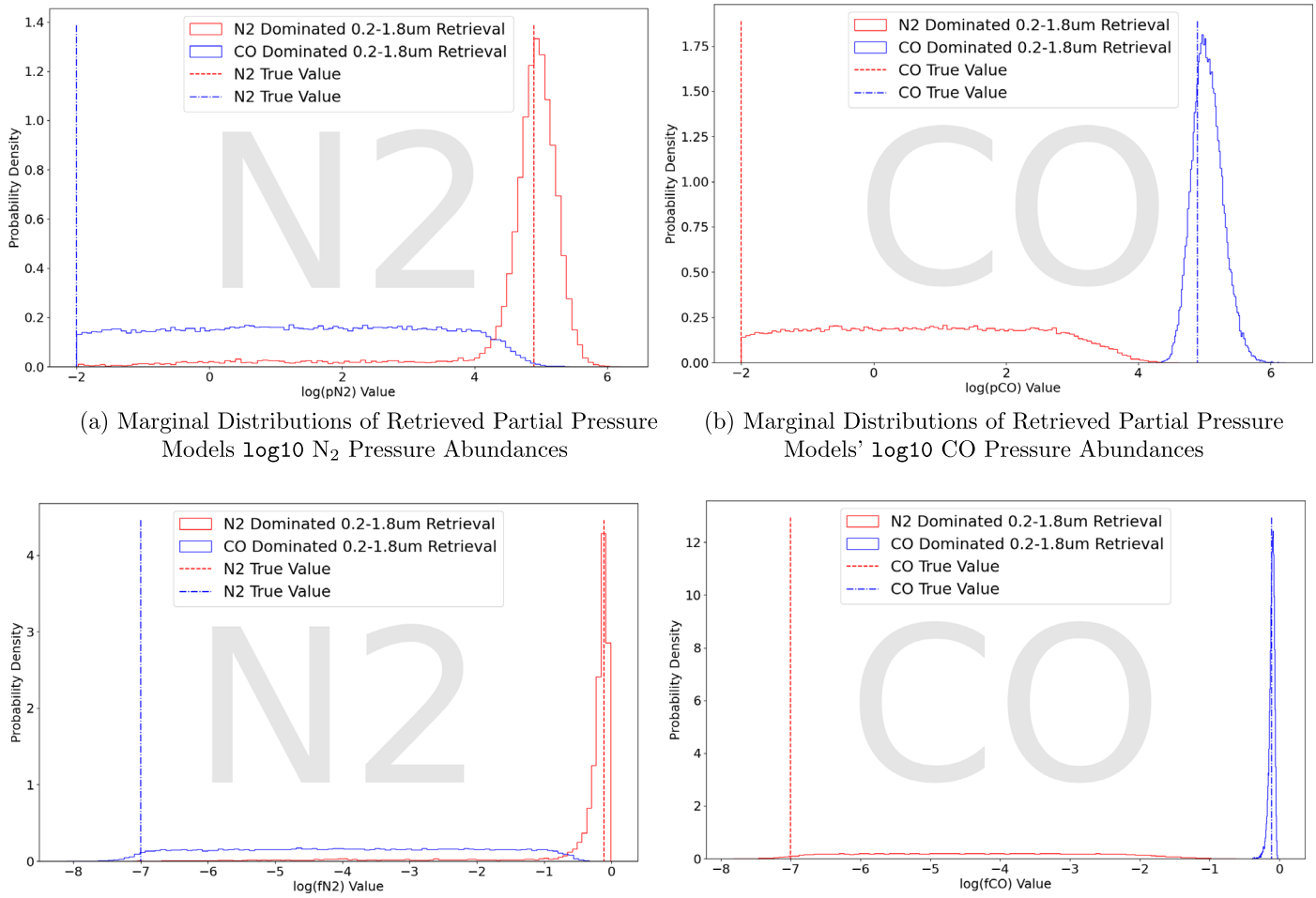

(a) Marginal Distributions of Retrieved Partial Pressure Models `log10` N_2 Pressure Abundances

(b) Marginal Distributions of Retrieved Partial Pressure Models' `log10` CO Pressure Abundances

(c) VMR Values From Figure Above

(d) VMR Values From Figure Above

Figure 7. Top row (left to right) partial pressure retrieval model N_2 and CO posteriors. Bottom row (left to right) VMR adapted partial pressure retrieval model N_2 and CO posteriors. Red marginal distributions represent abundances from N_2-dominated retrievals and blue distributions represent abundances from CO-dominated retrievals. The gas' true value lines are overplotted for each retrieval illustrated with the same color as its retrieval. The left column presents N_2 abundances for both retrievals with CO abundances shown in the right column. Both models are able to constrain our defined background gas and the trace gas has an abundance ceiling that trades with the background gas.

N_2-dominated and CO-dominated 0.2–1.1 μm confidence intervals).

3.5. Sensitivity to Assumed S/N

One important consideration for mission design is determining what S/Ns are required for a future telescope to distinguish gas species and their abundances. We ran three retrievals at different representative S/Ns (with otherwise nominal parameter choices) to investigate the minimum S/N required for a telescope to constrain the background gas: S/N = 10, 20, and 40 (Figure 10).

Recall that there was a degeneracy between O_2- and N_2-dominated atmospheres in the nominal S/N = 20 retrieval presented previously (e.g., Figure 3). This results in a slightly bimodal oxygen VMR marginal posterior (e.g., Figure 4). While the probability (P) of an O_2-dominated atmosphere is low for S/N = 20 retrievals ($P = 21.86\%$ for O_2 VMR > 0.5 and $P = 11.12\%$ for O_2 VMR > 0.8), the O_2–N_2 background degeneracy is resolved at higher S/N observations. At S/N = 40, the probabilities of an O_2-dominated atmosphere drop sharply ($P = 0.43\%$ for O_2 VMR > 0.5 and $P = 0.0\%$ for O_2 VMR > 0.8).

Figure 10 presents the gas-only corner plots of our S/N = 10, 20, and 40 N_2-dominated partial pressure retrievals. Figure 10(a) illustrates S/N = 10 retrieval results. 3σ contours qualitatively differ from the 2σ distributions of gas values for the S/N = 20 case. Crucially, N_2 and CO abundances covary and an N_2 background cannot be confidently detected at S/N = 10. Figure 10(b) shows that S/N = 20 results dramatically improve upon the S/N = 10 limitations. Figure 10(c) shows that S/N = 40 provides the tightest constraints on background atmospheric abundances. The low probability degeneracy between an N_2 and O_2 background is completely resolved at S/N = 40. Retrieved spectra and confidence intervals for the S/N = 10, 20, and 40 cases are shown in the Supplementary Materials.

4. Discussion

The ability to constrain background gas abundances is important for ruling out O_2 biosignature false positives and for assessing planetary climate. For temperate, Earth-analog planets, H_2O photolysis, and subsequent H escape are typically limited by cold trapping of water vapor in the lower atmosphere. However, small non-condensible (e.g., N_2, CO_2, CO) background

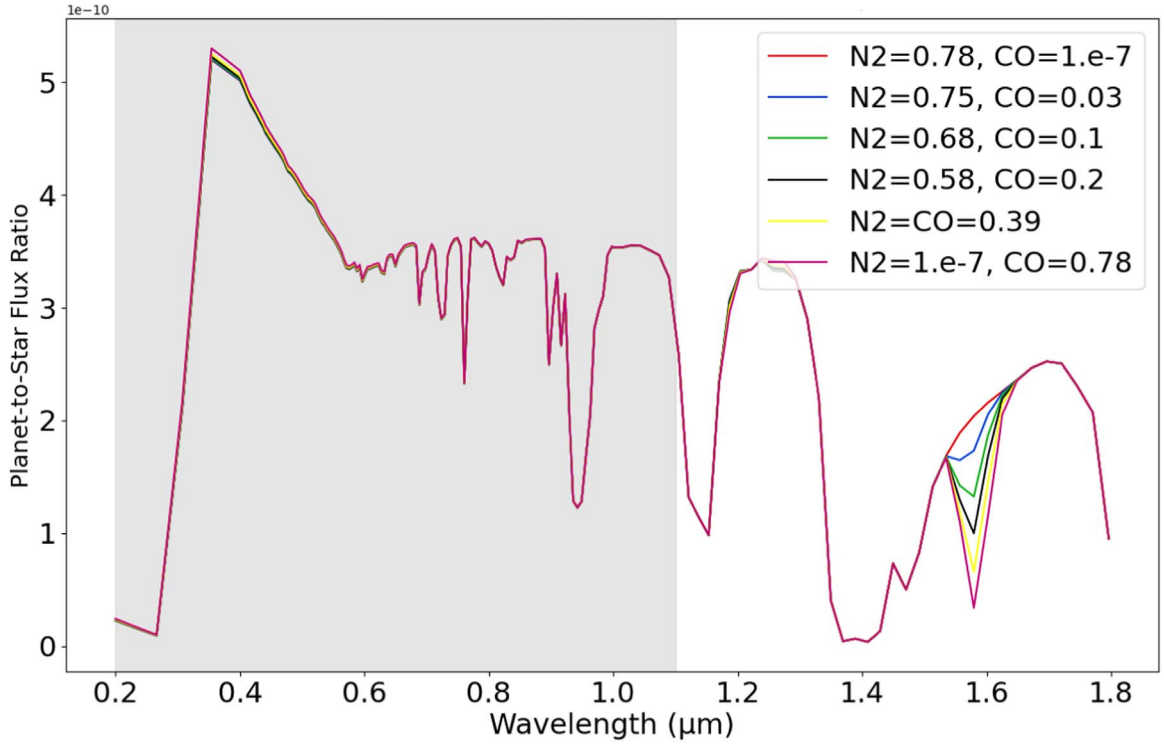

Figure 8. Comparison of the nominal N_2-dominated atmosphere and trading off VMRs of CO with N_2. The $\sim$1.6 μm CO absorption feature is needed to distinguish between N_2 and CO backgrounds.

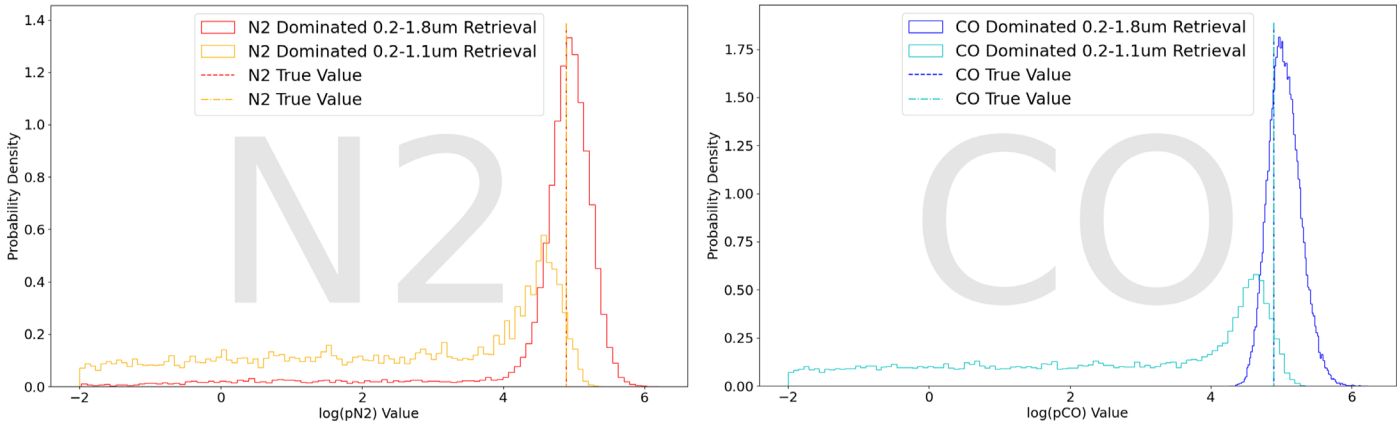

(a) Marginal Distributions of 0.2-1.1 μm vs. 0.2-1.8μm Partial Pressure Retrieval N_2 Posteriors

(b) Marginal Distributions of 0.2-1.1 μm vs 0.2-1.8μm Partial Pressure Retrieval CO Posteriors

Figure 9. N_2 (left) and CO (right) retrieved partial pressures comparing the 0.2–1.8 μm to the 0.2–1.1 μm wavelength ranges. Figure 9(a) presents our N_2 abundances for our 0.2–1.8 μm N_2-dominated retrievals in red and our 0.2–1.1 μm N_2-dominated retrievals in yellow. Both N_2-dominated retrievals have an N_2 abundance true value of 78% of the total atmosphere. Vertical lines show N_2's true value using the same color code. Similarly, Figure 9(b) presents our CO abundances for our 0.2–1.8 μm CO-dominated retrievals in blue and our 0.2–1.1 μm CO-dominated retrievals in cyan. Both CO-dominated retrievals have a CO abundance true value of 78% of the total atmosphere. Vertical lines show CO's true value using the same color code. Without extended wavelength coverage, our model is unable to differentiate N_2 from CO and they share similar abundances that fall outside of their true value.

inventories can lead to elevated H_2O abundances in the upper atmosphere, resulting in significant abiotic O_2 accumulation on geologic timescales (Wordsworth & Pierrehumbert 2014). While the simulated constraints in this study on background N_2 and total pressure are crude, they are sufficient to strongly disfavor an extreme H-loss scenario caused by a negligible ($\ll$1 bar) N_2 non-condensible background. Moreover, our simulations suggest that N_2 and CO backgrounds can be confidently distinguished from $S/N = 20$ with achievable resolutions $R = 7$, 140, and 70 for wavelength ranges 0.2–0.4 μm, 0.4–1.0 μm, and 1.0–1.8 μm respectively. Even for observations at more restricted wavelength ranges (0.2–1.1 μm), all other plausible backgrounds (H_2O, CO_2, O_2, CH_4) can be ruled out, although the degeneracy between N_2- and CO-dominated atmospheres cannot be broken without spectral coverage including CO absorption at 1.6 μm. This suggests that NIR wavelength capabilities will be crucial for interpreting any O_2 detection with next-generation direct imaging observations.

Constraints on total pressure, particularly lower limits, may indirectly provide additional evidence against an oxygen false-

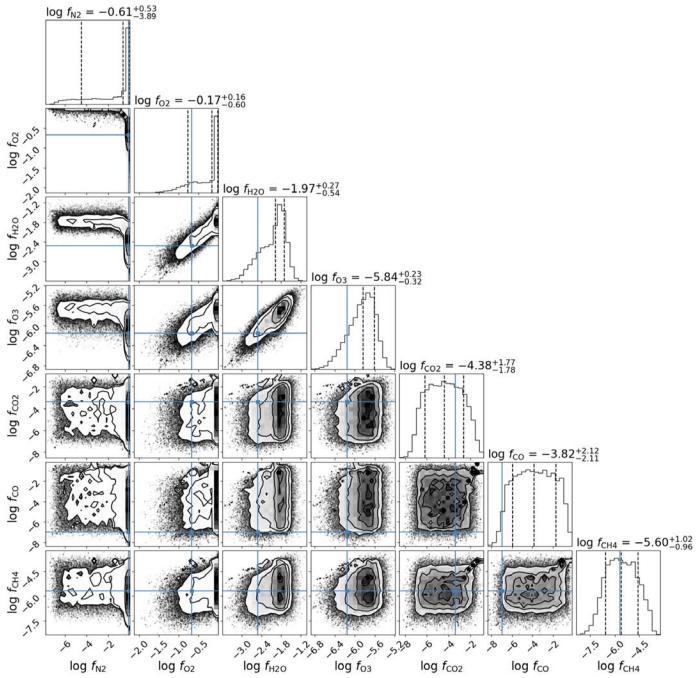

(a) SNR=10 Corner Plot in `log10` VMR Values

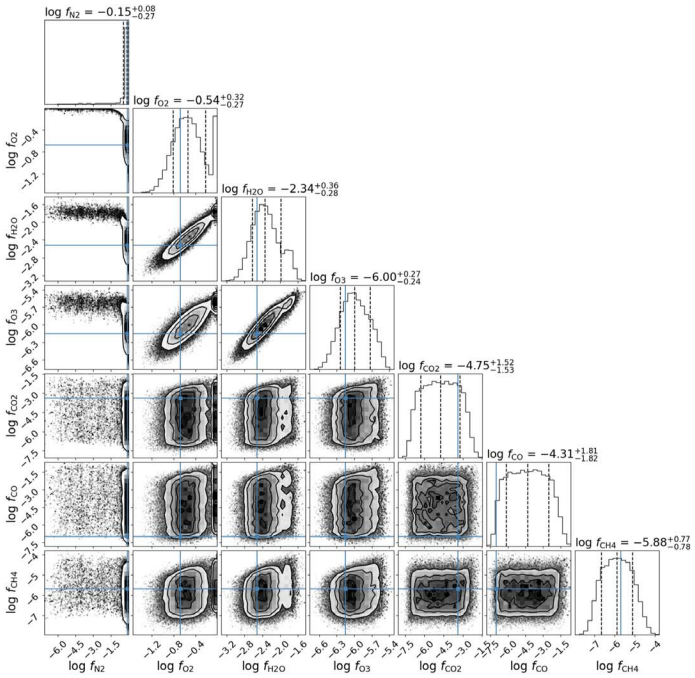

(b) SNR=20 Corner Plot in `log10` VMR Values

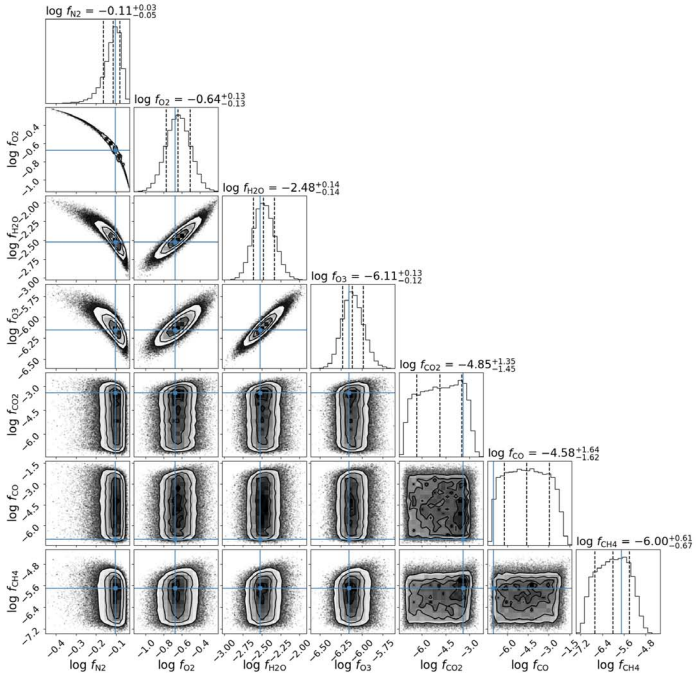

(c) SNR=40 Corner Plot in `log10` VMR Values

Figure 10. Corner plots for our partial pressure retrievals at S/N 10, 20, and 40. All plots are shown with the gas' `log10` VMR values in Pa.

positive scenario, even if individual abundances are poorly constrained. This is because the oxygen accumulation scenario envisaged in Wordsworth & Pierrehumbert (2014) is self-limiting—for a pure steam atmosphere, oxygen accumulation from hydrogen escape will itself become the non-condensible background gas, limiting oxygen accumulation at around 0.2 bar. Thus, constraining total pressure to >0.2 bar would add weight to the argument that oxygen is biological. For nominal calculations, retrieved total pressure is inferred to exceed 0.2 bar with 99.99997% confidence. This total pressure constraint is particularly useful for intermediate pressure cases where breaking the N_2–O_2 degeneracy is more challenging. For example, we conducted a sensitivity test where total pressure = 0.4 bar but mixing ratios were otherwise the same as the nominal retrieval. Here, the N_2–O_2 degeneracy cannot be broken, even at S/N = 40. However, total pressure is inferred to be >0.2 bar with 96.2% confidence (S/N = 20) and 99.3% confidence (S/N = 40). It should be noted however, that total

Table 3
Hours to Achieve S/N = X at $R = 70$ for a Planet 10 pc Away

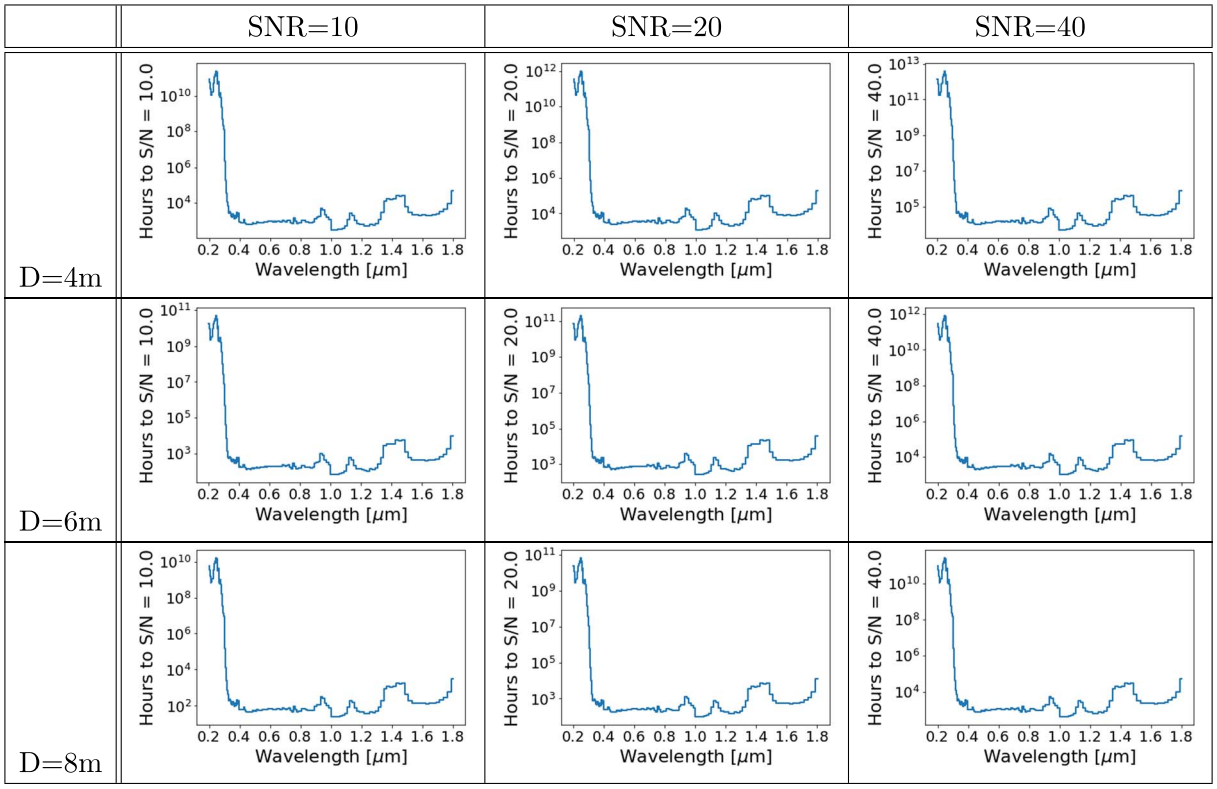

pressure alone does not unambiguously rule out an oxygen false positive since the precise self-limiting pressure threshold is potentially dependent on planet size, age, other trace constituents, redox evolution, etc.

4.1. Observing Times and Telescope Apertures Requirements

To illustrate the plausibility of obtaining observations with sufficient S/N and resolution to identify background gases, we used the `coronagraph` Python package (Lustig-Yaeger et al. 2019) to estimate required integration times for plausible telescope properties. By supplying the model with telescope diameters and desired S/Ns, we calculated the observation duration in hours required to achieve the S/N given for each wavelength point.

Table 3 presents the resulting wavelength-dependent observation times required for an HWO-type telescope with resolution $R = 70$ to achieve specific S/Ns across the 0.2–1.8 μm wavelength range. The columns are separated into S/Ns of 10, 20, and 40 (left to right), and the rows are separated into telescope diameters of 4, 6, and 8 m (top to bottom). To achieve an S/N = 20 and $R = 70$ at 1.6 μm for a planet 10 pc away, a 4 m telescope requires ~8000 hr of observation time, a 6 m telescope requires ~1600 hr, and an 8 m telescope requires ~560 hr. The average observation time required to achieve an S/N = 20 and $R = 70$ in the 1.0–1.8 μm wavelength range for a planet 10 pc away is ~19,000 hr for 4 m telescopes, ~4000 hr for 6 m telescopes, and ~1400 hr for 8 m telescopes. For reference, the Hubble Ultra Deep Field required 550 hr of integration time. Note that the required exposure time can be reduced by integrating spectral information over its wavelength range and will depend on details like detector noise properties and the number of exozodis in the system. The requisite exposure time for gas features that span N spectral elements will (to first order) scale as $1/\sqrt{N}$. For example, if the CO spectral impact spans four spectral elements, there is a factor of ~2 reduction in exposure time from integrating across the band.

The same process used for Table 3 was also applied to Table 4, except $R = 140$ across the entire 0.2–1.8 μm wavelength range. This wavelength range is important for identifying O_2, H_2O, O_3, CO_2, and CH_4 spectral features and constraining their abundances. At $R = 140$ the average observation time required to achieve S/N = 20 within the 0.4–1.0 μm wavelength range is ~14,000 hr for a 4 m telescope, ~2900 hr for a 6 m telescope, and ~980 hr for an 8 m telescope. While obtaining the longer requisite exposure times at these NIR wavelengths would be challenging, a *deep dive* to try to rule in/out CO would likely be reserved for only key targets. Note also, however, that because the inner working angle (IWA) grows linearly with wavelength for coronagraphs, more distant planets could be lost inside the IWA at these longer NIR wavelengths unless the telescope is larger. For more distant targets, larger apertures would be necessary to enable high enough angular resolution at long wavelengths to see the CO absorption feature at 1.6 μm.

Table 4
Hours to Achieve S/N = X at $R = 140$ for a Planet 10 pc Away

	SNR=10	SNR=20	SNR=40
D=4m	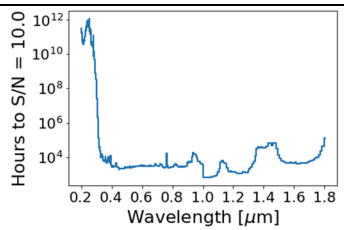	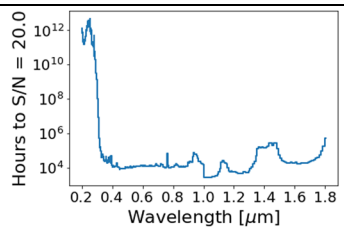	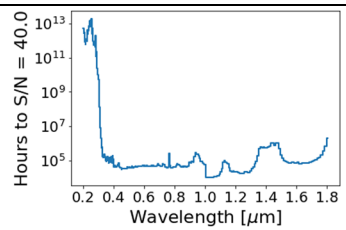
D=6m	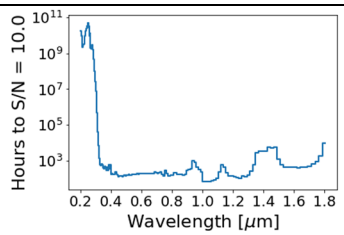	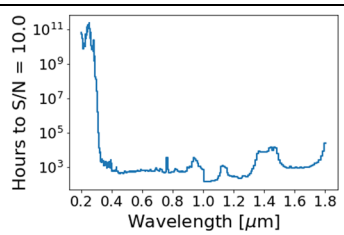	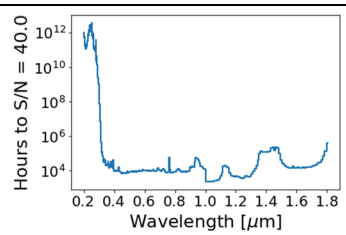
D=8m	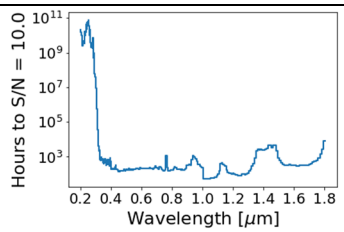	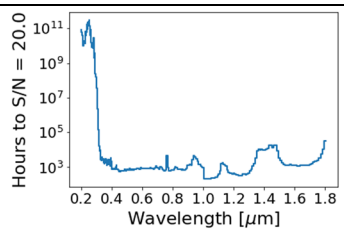	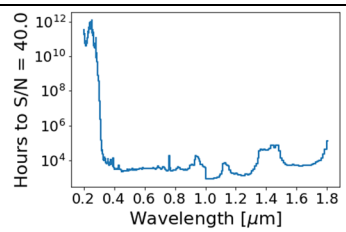

Taken as a whole, these integration time calculations suggest that large apertures (∼8 m) may be necessary to completely break the N_2–O_2 degeneracy and rule out oxygen biosignature false positives due to low non-condensible gas inventories.

4.2. Caveats and Perspectives

Our work in this paper consisted of simulated reflected light retrievals at constant, full phase. Realistic observations would be phase dependent and future work could explore whether observations over different phases could break degeneracies and provide better pressure information to determine background pressure with greater precision via time-variable Rayleigh scattering. In addition, the cloud model consists of water ice and liquid clouds with realistic wavelength-dependent scattering properties and a Henyey–Greenstein phase function. Future work should additionally include wavelength-dependent aerosol absorption for more accurate results.

More broadly, our radiative transfer and retrieval calculations neglect shortwave absorption due to aerosols. This is justified on the grounds that oxygen-rich atmospheres (with water vapor) are unlikely to be hazy due to the oxidation of haze-forming species by OH radicals. The omission of shortwave haze absorption is also unlikely to affect our conclusions regarding disentangling N_2 and CO backgrounds since NIR absorption is used to distinguish these gases. However, future work ought to explore the possible influence of hazes on constraining background pressure via the Rayleigh tail, and possible degeneracies introduced by this.

The calculations presented in this paper conservatively assume N_2 pressure broadening in all cases. In reality, CO pressure broadening may help distinguish N_2- and CO-dominated atmospheres. Future experiments or theoretical work to accurately compute CO pressure broadening could be incorporated into simulated retrievals to determine if differential pressure broadening significantly affects reflected light spectra.

For this work, we have assumed on cosmochemical grounds that Ar, Ne, and other non-condensibles are negligible terrestrial atmospheric background gases. However, the diversity of terrestrial planet atmospheres is unknown, and planetary composition does not scale directly with cosmochemical abundances, nor does atmospheric composition necessarily scale with bulk planet composition. Earth's dry atmosphere contains an Ar mixing ratio of ∼1% (higher than CO_2, CO, CH_4), resulting primarily from the cumulative radioactive decay of ^{40}K over geologic time. For planets with larger inventories of ^{40}K and/or older planets with more time for radioactive decay, higher ^{40}Ar mixing ratios are conceivable (although the increased heat production and outgassing from enhanced interior heating likely correlates with C, H, and/or N degassing). Scenarios where atmospheric Ar is a significant portion of an ∼0.2 bar atmosphere are conceivable. Future work ought to explore the geochemical plausibility and detectability of these alternative background gases, especially those that are non-absorbing in the UV–visible-NIR.

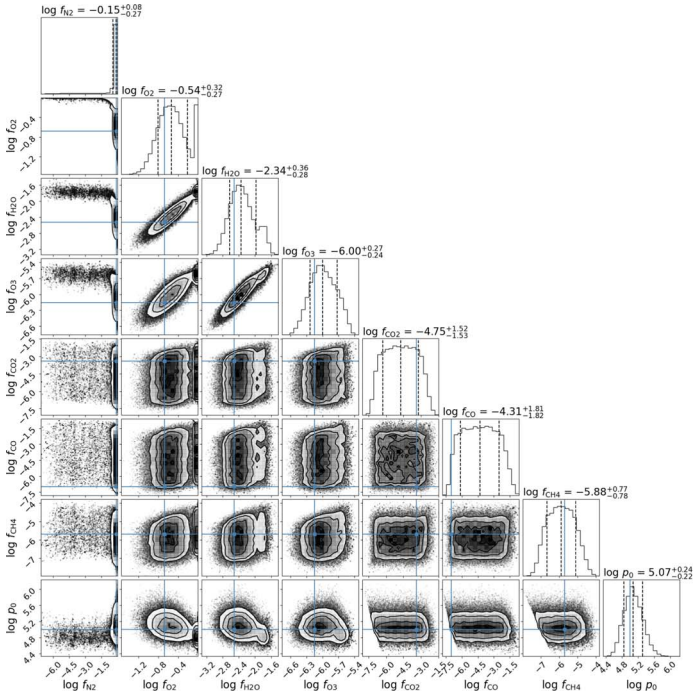

(a) N_2-Dominated Partial Pressure Retrieval Gases Shown With Their VMR Values Plotted Against Total Atmospheric Pressure

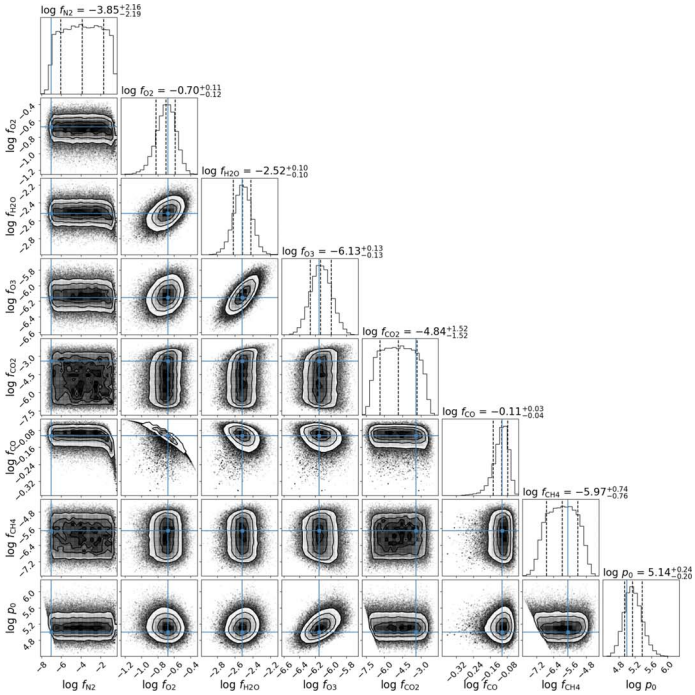

(b) CO-Dominated Partial Pressure Retrieval Gases Shown With Their VMR Values Plotted Against Total Atmospheric Pressure

Figure 11. Gas-pressure corner plots of N_2-dominated (left) and CO-dominated (right) partial pressure retrievals with gas values shown as mixing ratios.

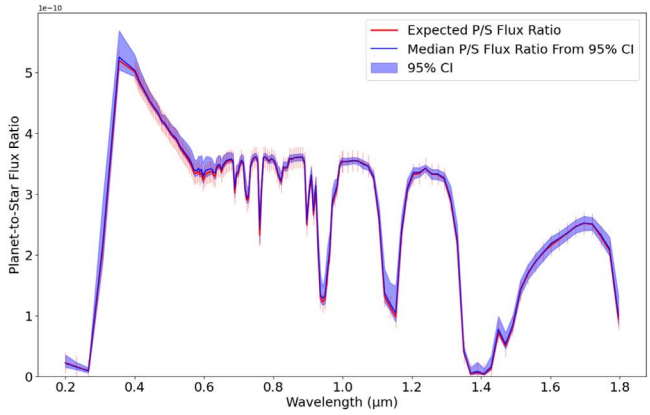

(a) N_2-CO Swap Partial Pressure Retrieval True Spectrum vs. 1000 Model Spectra w Confidence Interval

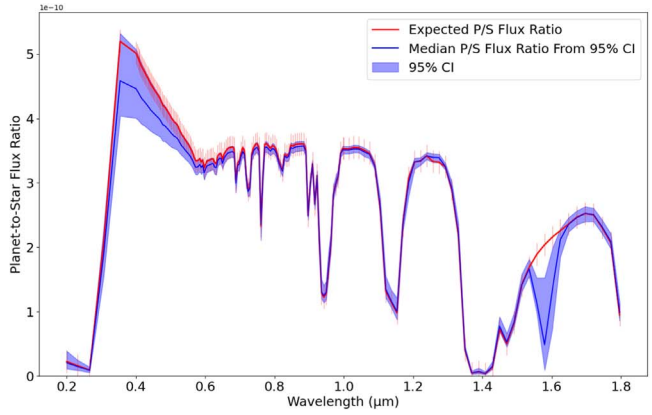

(b) N_2-CO Swap VMR Retrieval True Spectrum vs. 1000 Model Spectra w Confidence Interval

Figure 12. Spectra confidence intervals for N_2–CO swap retrievals. Although both retrievals had true values of $N_2 = 0.78$ and $CO = 1.e{-}7$, only the partial pressure retrieval was able to calculate accurate results. We see the N_2–CO VMR retrieval sampled many iterations with a high CO abundance evidenced by the absorption feature at $\sim$1.6 μm.

The swapped N_2–CO abundances retrieval we conducted to explore the N_2–CO degeneracy is a somewhat artificial test case. Such a situation is photochemically unlikely because abundant CO was likely sourced from CO_2 photolysis, and so a higher background CO_2 abundance is to be expected. Conversely, even in the absence of outgassed CO_2, CO may be photochemically oxidized to CO_2. Thus, another test case we considered is the plausibility of atmospheres with both high CO and CO_2 to investigate whether the CO–N_2 degeneracy could be broken in the presence of strong CO_2 absorption features. Specifically, CO's only significant spectrally active band in the relevant wavelength range ($\sim$1.6 μm) overlaps with a CO_2 absorption feature, and so high levels of CO could possibly be hidden by relatively moderate abundances of CO_2, worsening the CO–N_2 degeneracy.

To test the plausibility of a HWO breaking CO–CO_2(–N_2) degeneracies, we ran retrievals using the photochemically self-consistent atmospheres in Gao et al. (2015) at both $S/N = 20$ and 40. Instrument and atmospheric parameters were otherwise the same as the nominal case except with revised VMRs as follows:

$N_2 = 0.02$

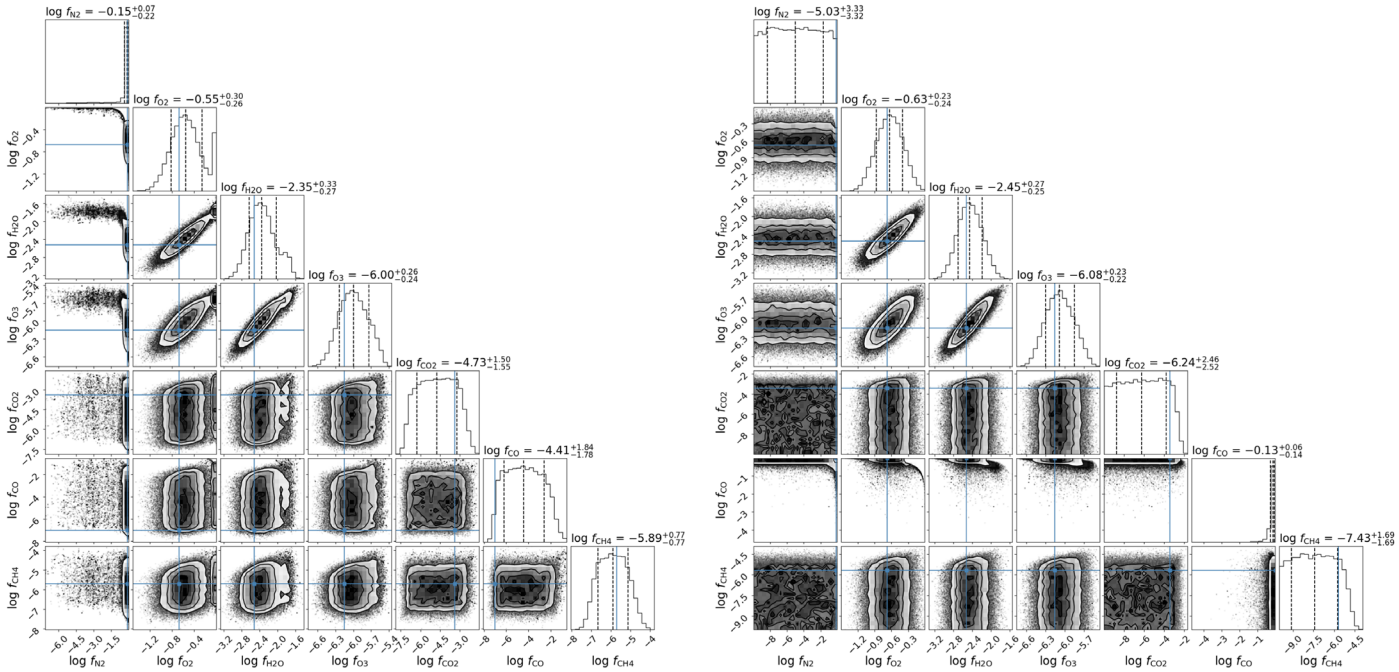

(a) N_2-CO Swap Partial Pressure Retrieval Gas Only Corner Plot shown w `log10` VMR Values For Easier Comparison

(b) N_2-CO Swap VMR Retrieval Gas Only Corner Plot

Figure 13. N_2–CO swap retrieval corner plots. The VMR retrieval could not constrain either N_2 or CO accurately for the swapped case.

O_2 = 0.17
H_2O = 4.e-9
O_3 = 7.e-8
CO_2 = 0.45
CO = 0.35
CH_4 = 1.e-7.

We found that even for these high CO+CO_2 atmospheres, a CO–CO_2 background can be inferred with high confidence and distinguished from an N_2 background (not shown). Specifically, at S/N = 40, a CO mixing ratio of less than ∼0.22 is excluded with 84% confidence (and VMR < 0.17 is excluded with 95% confidence) while the CO_2 mixing ratio is found to exceed 0.42 with 84% confidence (and CO_2 VMR > 0.37 with 95% confidence). Moreover, O_2 VMRs can be constrained with high precision even at S/N = 20. Introducing abundant CO_2 does not dramatically change our conclusions because the peak CO_2 and CO absorption around 1.6 μm are offset from one another, allowing the two species to be distinguished.

Our work investigated the potential of an HWO to constrain background gas abundances to rule out one type of O_2 false positives for Earth analogs following Wordsworth & Pierrehumbert (2014). Future work could convolve simulated N_2 partial pressure constraints with atmospheric models of H_2O cold trapping and H escape to determine the extent to which future observations would confidently exclude abiotic oxygen. Additional opportunities for future work include performing retrievals to rule out other O_2 biosignature false positives for high CO_2 runaway greenhouse atmospheres (Krissansen-Totton et al. 2021), or waterworld false positives (Krissansen-Totton et al. 2021).

5. Conclusion

Distinguishing background gases and constraining their abundance can inform assessments of planetary climate and help determine whether O_2 in an exoplanet's atmosphere is of biotic or abiotic origin. Our results suggest that distinguishing background N_2 from CO and other gases is possible, even for wavelength ranges where N_2 has no distinguishable absorption spectral features. This is because all other plausible terrestrial planet background gas constituents absorb in the optical and NIR, and thus can be ruled out as dominant constituents based on the lack of absorption features. Yet, it is important that telescopes like HWO possess wavelength ranges including the CO ∼1.6 μm absorption feature, which is clearly visible at $R = 70$ with an S/N = 20. Additionally, the HWO's observational wavelength range must extend past the CO absorption feature in order to accurately constrain CO abundance, which can then (in combination with total pressure constraints from the Rayleigh slope and gas absorption features) be used to constrain N_2 within a wavelength range of 0.2–1.8 μm. These observations are feasible given plausible integration times. Specifically, an 8 m diameter telescope requires only 560 hr, or ∼1/3 the observation time required by a 6 m telescope (1600 hr) with $R = 70$ to achieve a sufficient S/N of 20 at the 1.6 μm CO absorption feature for an Earth analog at 10 pc.

Bimodal O_2 abundance posteriors were obtained for our N_2-dominated retrievals, indicating a very low probability of an O_2-dominated atmosphere appearing as an N_2-dominated atmosphere. However, this O_2–N_2 is broken at higher S/Ns; for S/N = 20 partial pressure retrievals 21.86% of iterations had an O_2 VMR > 0.5 and 11.12% of iterations had an O_2 VMR > 0.8, for S/N = 40 retrievals 0.43% of iterations had an O_2 VMR > 0.5 and no iterations had an O_2 VMR > 0.8.

Acknowledgments

We thank the UCSC Koret Scholars Program for funding S.H. J.K.T. was supported by the NASA Sagan Fellowship and

through the NASA Hubble Fellowship grant HF2-51437 awarded by the Space Telescope Science Institute, which is operated by the Association of Universities for Research in Astronomy, Inc., for NASA, under contract NAS5-26555. This work was additionally supported by NASA Astrophysics Decadal Survey Precursor Science grant 80NSSC23K1471. Finally, we would like to thank the anonymous reviewer, Edward Schwieterman, and the UC Santa Cruz exoplanet squad for their helpful suggestions and critiques. T.D.R. gratefully acknowledges support from NASA's Exoplanets Research Program (No. 80NSSC18K0349) and Exobiology Program (No.80NSSC19K0473), the Nexus for Exoplanet System Science Virtual Planetary Laboratory (No. 80NSSC18K0829), and the Cottrell Scholar Program administered by the Research Corporation for Science Advancement. A.S. and T.D.R. gratefully acknowledge support from NASA's Habitable Worlds Program (No. 80NSSC20K0226).

Appendix
Supplemental Material

A.1. Constraining Total Pressure and Background Gas Composition

By retrieving gas partial pressures, our atmospheric species abundances were independent of each other and of total atmospheric pressure. To calculate our total atmospheric pressure then, we simply summed the retrieved abundances of our atmospheric gases such that

$$\mathtt{pmax} = \mathtt{pN_2} + \mathtt{pO_2} + \mathtt{pH_2O} + \mathtt{pCO_2} + \mathtt{pO_3} + \mathtt{pCO} + \mathtt{pCH_4}.$$

Since total atmospheric pressure is a feature with spectral ramifications (see the Supplemental Material), we are able to constrain our total atmospheric pressure via the summation of our gas abundances.

From our N_2-dominated retrievals, we see a strong N_2–O_2 tradeoff feature in our mixing ratio corner plots. There is additionally a low probability of our model retrieving an O_2-dominated atmosphere with small N_2 abundances. This O_2–N_2 degeneracy presents itself in atmospheres lighter than the median pressure expected from an N_2-dominated atmosphere. O_2 spectral features constrain O_2 abundance directly, correlating lower total pressures with low N_2 mixing ratios. The degeneracy can be seen in the $\mathtt{O_2}$-pmax 2D covariant posterior in Figure 11(a). This degeneracy was not seen in CO-dominated atmospheres, which prefer slightly heavier atmospheres, and Figure 11(b) illustrates that concept.

A.2. Retrieving Partial Pressures versus Retrieving VMRs

Throughout the course of our retrievals, we tested our gas abundance retrievals in two ways: (1) retrieving partial pressure abundances of our gases such that they are independent of each other's values and the total atmospheric pressure is the sum of all constituent partial pressures, and (2) retrieving VMR values of the gases such that they are ratios of the total atmospheric pressure that must sum to 1. The VMR retrieval case coupled the gas abundances with the atmospheric pressure, and since N_2 is radiatively inactive in the 0.2–1.8 μm wavelength range, its abundance was inferred as the difference between unity and the other gas abundances such that

$$\mathtt{fN_2} = 1 - (\mathtt{fO_2} + \mathtt{fH_2O} + \mathtt{fO_3} + \mathtt{fCO_2} + \mathtt{fCO} + \mathtt{fCH_4}).$$

Contrary to our VMR retrieval method, by retrieving partial pressure abundances of our gases we could ensure the retrieval was not biased toward backfilling the atmosphere with any particular gas:

$$\mathtt{pmax} = \mathtt{pN_2} + \mathtt{pO_2} + \mathtt{pH_2O} + \mathtt{pCO_2} + \mathtt{pO_3} + \mathtt{pCO} + \mathtt{pCH_4},$$

where $\mathtt{pN_2}$, $\mathtt{pO_2}$, $\mathtt{pH_2O}$, $\mathtt{pCO_2}$, $\mathtt{pO_3}$, $\mathtt{pCO}$, and $\mathtt{pCH_4}$ values are initialized within their defined prior range (Table 1) then iterated through during the course of the retrieval.

Although both retrieval methods produced results that were superficially consistent with our true spectra and had confidence intervals that fit within error bars, closer investigation revealed that the VMR retrieval approach was biased toward our predefined background gas. We ran VMR and partial pressure retrievals where our forward model was given N_2 and CO VMR abundances of `0.78` and `1.e-7`, respectively. Then for our retrieval, we defined CO as our background gas and we swapped the MCMC chain initializations of N_2 and CO to see if our models would still be able to find the true value of those gases' abundances.

Figure 12 illustrates the two confidence intervals produced for the N_2–CO swap retrievals, with Figure 12(a) displaying results from the partial pressure retrieval and Figure 12(b) displaying results from the VMR retrieval. We can see that for the partial pressure retrieval, our confidence interval follows the true spectrum very well, similar to our nominal N_2-dominated partial pressure retrieval. Our VMR N_2–CO swap retrieval, however, shows our confidence interval contains many model runs with a high CO abundance, indicated by the 1.6 μm absorption feature.

Figure 13 displays the gas-only corner plots for our N_2–CO swap retrievals. Figure 13(a) presents the partial pressure retrieval, where the blue true value lines are within the 1σ contour of the 2D covariant plots and/or the covariant true values converge within the clouds of values. Figure 13(b) presents the VMR retrieval results. Even though N_2 had a true VMR of `0.78`, our model could not constrain it at all, and its value cloud spans the full range it was allowed to explore. Similarly, CO had a true VMR value of `1.e-7`, but has become our background gas with values centered around $10^{-0.13} = 0.74$. We see for both N_2 and CO, their blue true value lines are not found within their 2D covariant plots of values in Figure 13(b).

Thus, we conclude that VMR retrievals should not be used unless the background gas has been confidently identified by previous observations. Backfilling creates a bias in priors that results in incorrect posteriors.

A.3. Supplementary Plots

Figure 14 shows the true and retrieved spectra for the restricted wavelength range sensitivity test described in Section 3.4. Figure 15 shows the true and retrieved spectra for the S/N = 10, 20, and 40 sensitivity test described in Section 3.5. Figure 16 shows the temperature sensitivity of reflected light spectra is negligible for the temperate planets we are considering. Figure 17 shows the full posterior distribution for retrieved parameters for the CO-dominated sensitivity test described in Section 3.3, and Figure 18 is identical to Figure 17 except that retrieved partial pressures have been converted to mixing ratios.

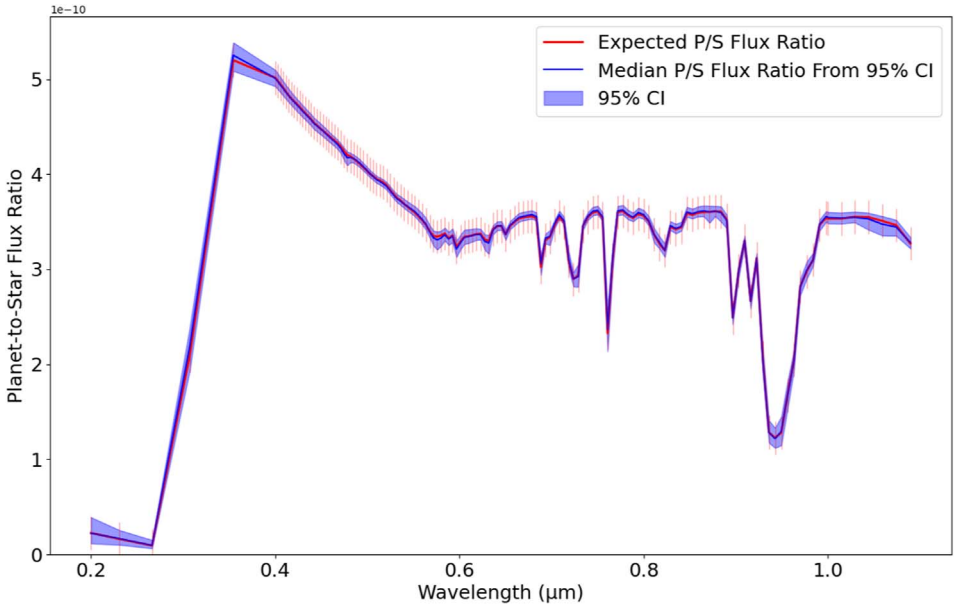

(a) N_2-Dominated 0.2-1.1 μm True Spectrum vs 1000 Retrieved Spectra w/ Confidence Interval

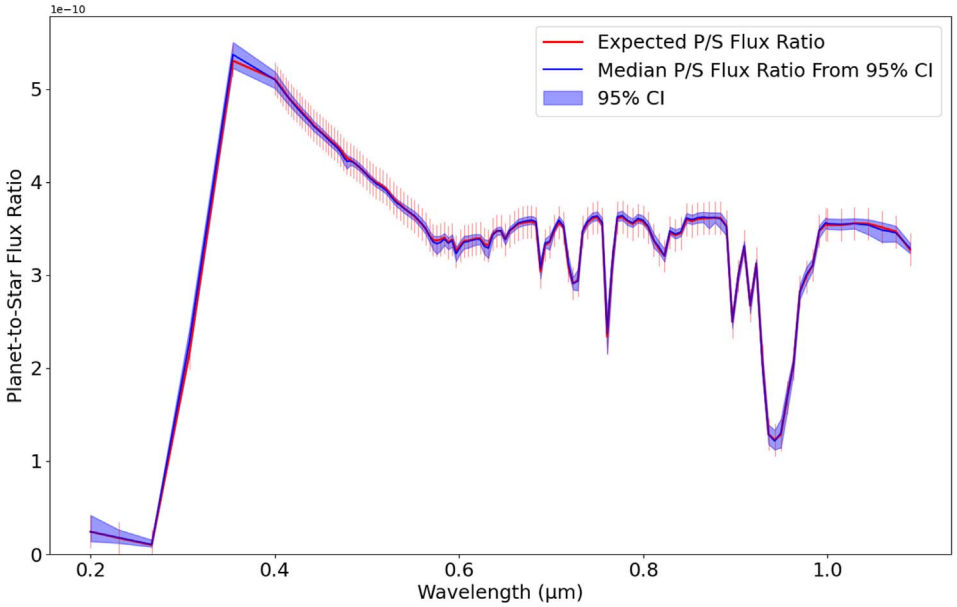

(b) CO-Dominated 0.2-1.1 μm True Spectrum vs 1000 Retrieved Spectra w/ Confidence Interval

Figure 14. True 0.2–1.1 μm N_2-dominated planet-to-star flux ratio spectrum (top) and CO-dominated spectrum (bottom) plotted against 1000 randomly sampled retrieved spectra with 95% confidence intervals.

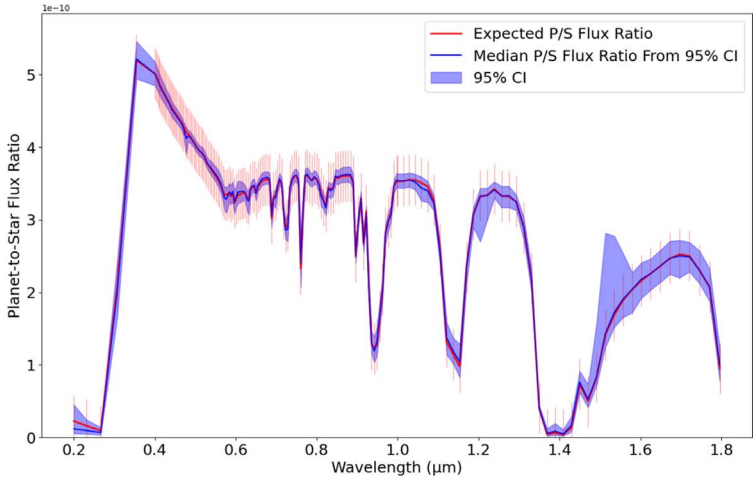

(a) True N_2-Dominated Spectrum vs. 1000 Randomly Sampled SNR=10 Retrieved Spectra

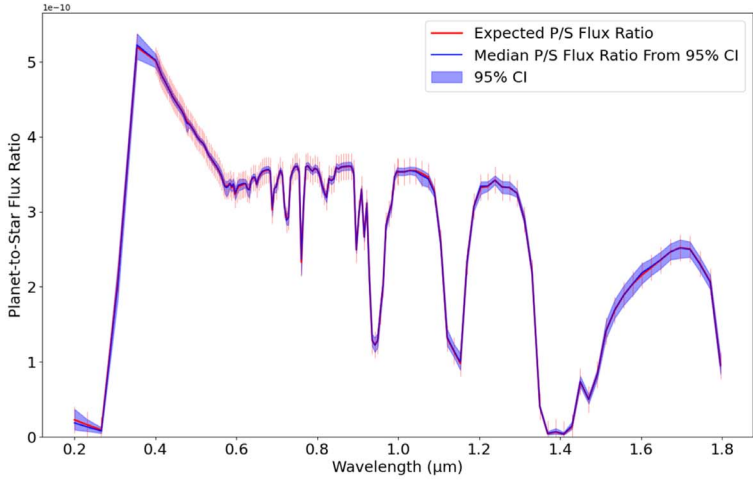

(b) True N_2-Dominated Spectra vs. 1000 Randomly Sampled SNR=20 Retrieved Spectra

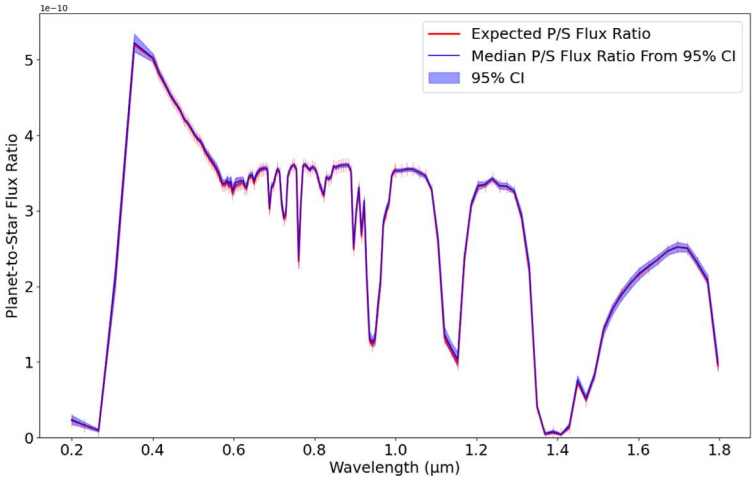

(c) True N_2-Dominated Spectra vs. 1000 Randomly Sampled PP SNR=40 Retrieved Spectra

Figure 15. N_2-dominated partial pressure retrievals' 95% confidence intervals with different S/Ns.

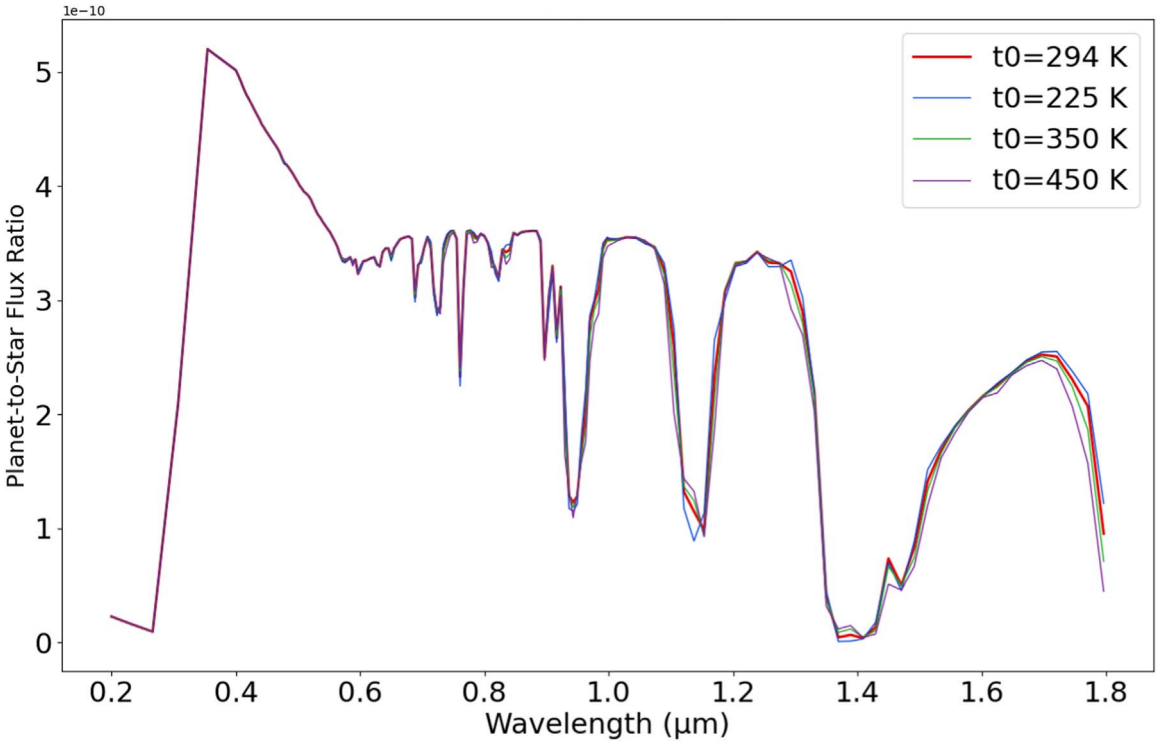

Figure 16. Spectra comparison of different surface temperatures on our observed exoplanet. Our nominal model fixes the temperature as outlined in Section 2, `t0 = 294 K`.

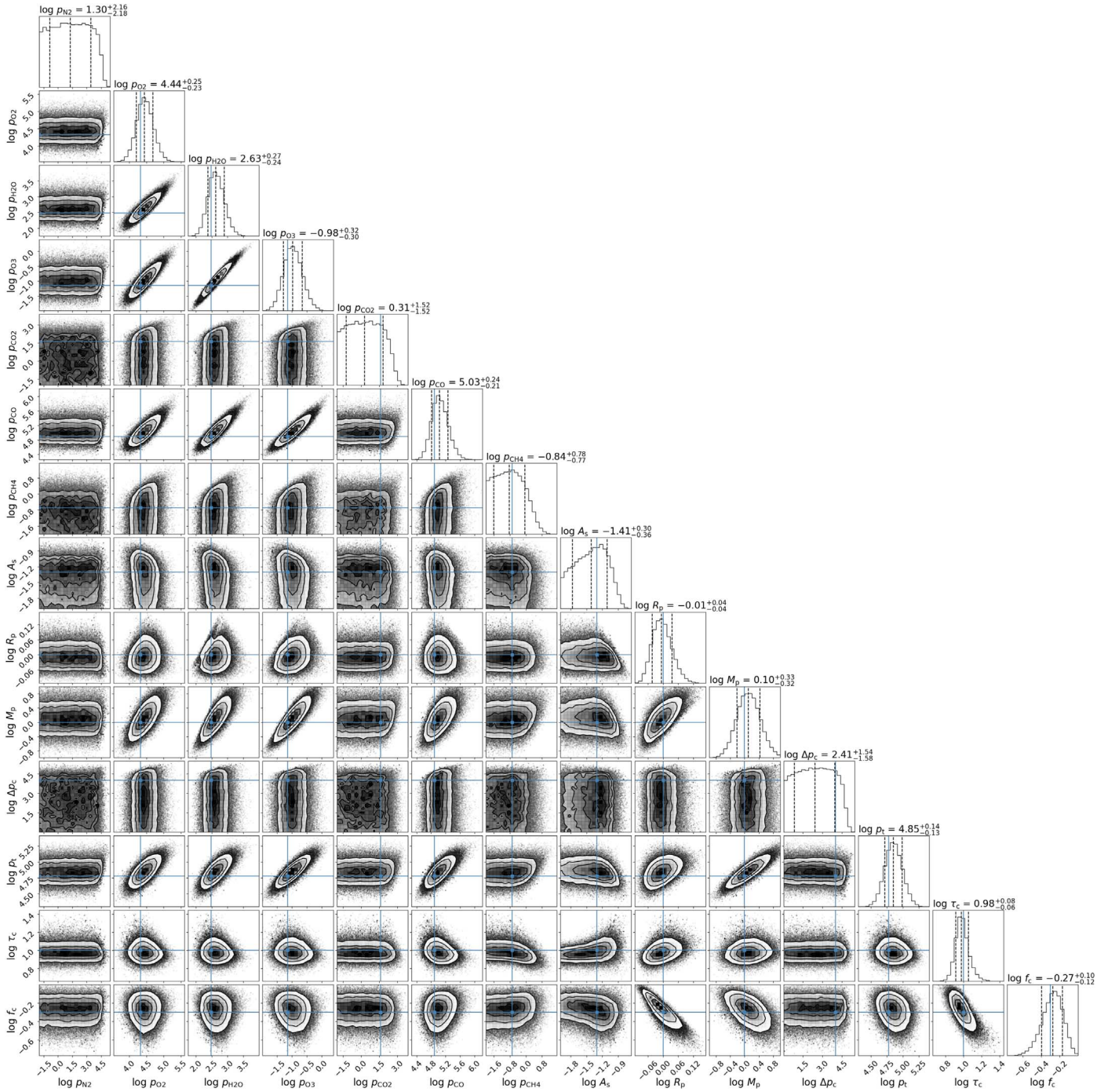

Figure 17. Partial pressure CO-dominated retrieval full corner plot.

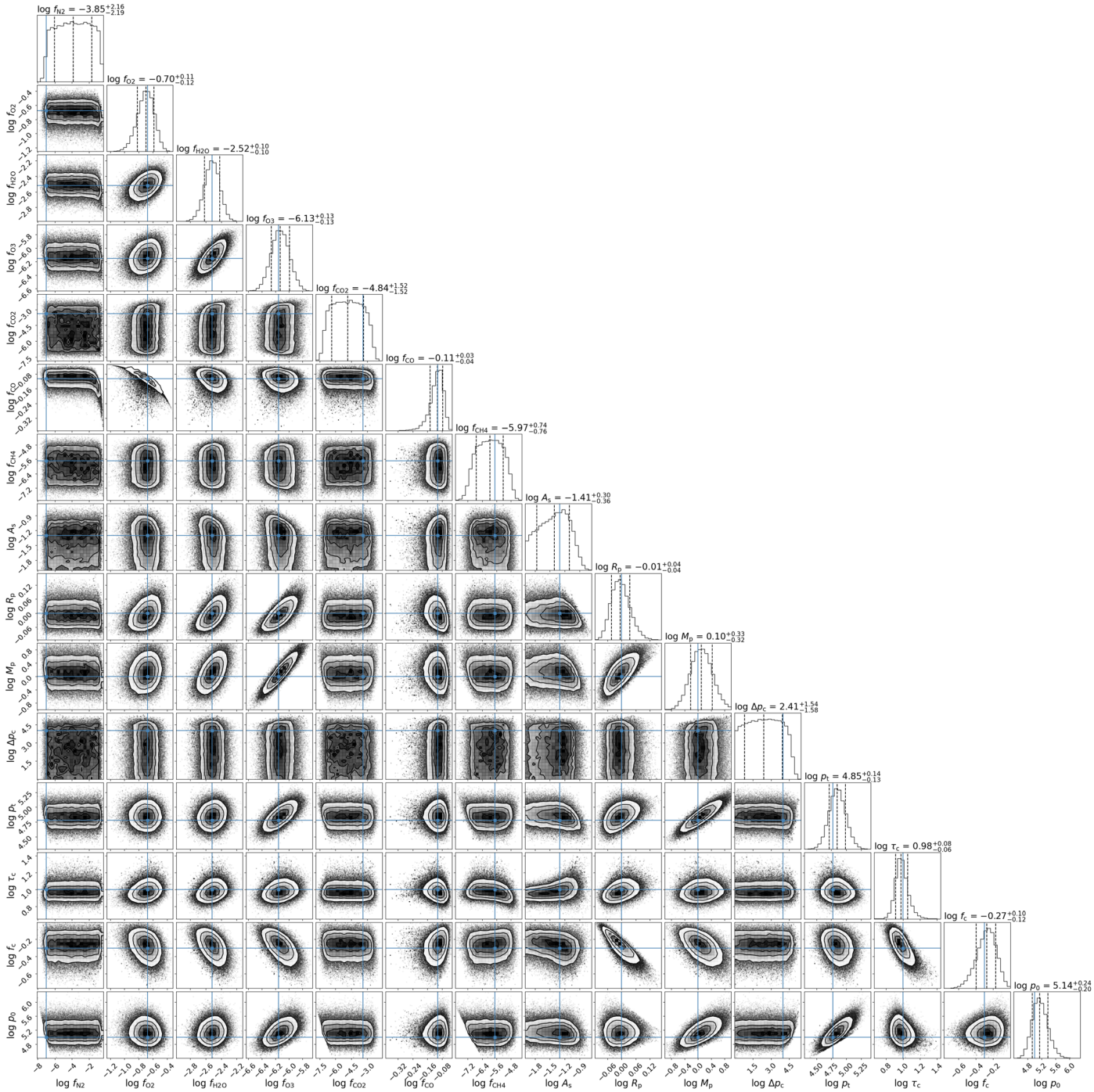

Figure 18. Partial pressure CO-dominated retrieval corner plot with gas abundances shown in their VMR values.

ORCID iDs

Sawyer Hall https://orcid.org/0000-0003-2070-5334
Joshua Krissansen-Totton https://orcid.org/0000-0001-6878-4866
Tyler Robinson https://orcid.org/0000-0002-3196-414X
Arnaud Salvador https://orcid.org/0000-0001-8106-6164
Jonathan J. Fortney https://orcid.org/0000-0002-9843-4354

References

Abrevaya, X. C., & Thomas, B. C. 2018, Habitability of the Universe Before Earth (New York: Academic Press), 27
Benneke, B., & Seager, S. 2012, ApJ, 753, 100
Damiano, M., & Hu, R. 2021, AJ, 162, 200
Damiano, M., & Hu, R. 2022, AJ, 163, 299
Feng, Y. K., Robinson, T. D., Fortney, J. J., et al. 2018, AJ, 155, 200
Foreman-Mackey, D., Hogg, D. W., Lang, D., & Goodman, J. 2013, PASP, 125, 306
Gao, P., Hu, R., Robinson, T. D., Li, C., & Yung, Y. L. 2015, ApJ, 806, 249
Gaudi, B. S., Seager, S., Mennesson, B., et al. 2020, arXiv:2001.06683
Goldblatt, C., Claire, M. W., Lenton, T. M., et al. 2009, NatGe, 2, 891
Gordon, I. E., Rothman, L. S., Hargreaves, R., et al. 2022, JQSRT, 277, 107949
Grenfell, J. L., Gebauer, S., Godolt, M., et al. 2018, ApJ, 861, 38
Harman, C. E., Schwieterman, E. W., Schottelkotte, J. C., & Kasting, J. F. 2015, ApJ, 812, 137
Hu, R., Peterson, L., & Wolf, E. T. 2020, ApJ, 888, 122

Johnson, B. W., & Goldblatt, C. 2018, GGG, 19, 2516
Kleinböhl, A., Willacy, K., Friedson, A. J., Chen, P., & Swain, M. R. 2018, ApJ, 862, 92
Krissansen-Totton, J., Fortney, J. J., & Nimmo, F. 2022, LPIC, 2687, 3021
Krissansen-Totton, J., Fortney, J. J., Nimmo, F., & Wogan, N. 2021, AGUA, 2, e00294
Lammer, H., Sproß, L., Grenfell, J. L., et al. 2019, AsBio, 19, 927
Luger, R., & Barnes, R. 2015, AsBio, 15, 119
Lustig-Yaeger, J., Robinson, T. D., & Arney, G. 2019, JOSS, 4, 1387
Meadows, V. S., & Crisp, D. 1996, JGRE, 101, 4595
Meadows, V. S., Reinhard, C. T., Arney, G. N., et al. 2018, AsBio, 18, 630
National Academies of Sciences, Engineering, and Medicine 2021, Pathways to Discovery in Astronomy and Astrophysics for the 2020s (Washington, DC: The National Academies Press)
Paradise, A., Fan, B. L., Menou, K., & Lee, C. 2021, Icar, 358, 114301
Robinson, T. D. 2022, hablabx/rfast: Initial Release (initial), Zenodo, doi:10.5281/zenodo.7327817
Robinson, T. D., & Salvador, A. 2023, PSJ, 4, 10
Robinson, T. D., Stapelfeldt, K. R., & Marley, M. S. 2016, PASP, 128, 025003
Schwieterman, E. W., Robinson, T. D., Meadows, V. S., Misra, A., & Domagal-Goldman, S. 2015, ApJ, 810, 57
Stüeken, E. E., Kipp, M. A., Koehler, M. C., & Buick, R. 2016, ESRv, 160, 220
The LUVOIR Team 2019, arXiv:1912.06219
Tian, F., France, K., Linsky, J. L., Mauas, P. J. D., & Vieytes, M. C. 2014, E&PSL, 385, 22
Wordsworth, R., & Pierrehumbert, R. 2014, ApJL, 785, L20
Wordsworth, R., Schaefer, L. K., & Fischer, R. A. 2018, AGUFM, 2018, P52A
Wordsworth, R. D. 2016, E&PSL, 447, 103
Zahnle, K., Haberle, R. M., Catling, D. C., & Kasting, J. F. 2008, JGRE, 113, E11004